TiS Trends in Sciences
TRENDS IN SCIENCES 2027; 24(1): 14541
SPRINT Scholarly Publishing and Repository Integration Center
https://doi.org/10.48048/tis.2027.14541
REVIEW ARTICLE

Recent Advances in BiOBr-based Materials Coupled with ZSM-5 as Potential Photocatalyst Composites for Environmental Remediation and Hydrogen Production: A Review

Revvara Khusuma[1], Wahyu Prasetyo Utomo[1,*], Nor Farida[1], Ade Irma Rozafia[1], Zjahra Vianita Nugraheni[1], Hao Wu[2], Zhi Zhu[3] and Djoko Hartanto[1]

[1]Department of Chemistry, Faculty of Science and Data Analytics, Institut Teknologi Sepuluh Nopember (ITS), Surabaya 60111, Indonesia
[2]Macao Institute of Materials Science and Engineering (MIMSE), Faculty of Innovation Engineering, Macau University of Science and Technology, Taipa 999078, China
[3]School of Chemistry and Chemical Engineering, Institute for Advanced Materials, Jingjiang College, Jiangsu University, Zhenjiang 212013, China

([*]Corresponding author's e-mail: wp.utomo@its.ac.id)

Received: 29 May 2026, Revised: 3 August 2026, Accepted: 17 August 2026, Published: 15 October 2026

Abstract

Increasing severity of organic pollution and the global demand for clean energy have stimulated extensive research into multifunctional photocatalytic systems capable of simultaneous environmental remediation and sustainable energy production. Among various semiconductor materials, bismuth oxybromide (BiOBr) has attracted significant attention due to its layered structure, internal electric field, and visible-light responsiveness. However, the practical application of pristine BiOBr remains limited by rapid charge recombination and restricted surface activity. Integrating BiOBr with porous zeolitic materials such as ZSM-5 has emerged as an effective strategy to overcome these limitations. ZSM-5 offers high surface area, excellent adsorption capability, and tunable acidity, enabling enhanced dispersion of BiOBr, improved pollutant pre-concentration, and facilitated interfacial charge transfer. This review provides a comprehensive discussion of recent advances in BiOBr and its combination with ZSM-5, focusing on the potential of BiOBr-based photocatalyst coupled with ZSM-5 for organic pollutant degradation and hydrogen evolution reaction. The fundamental aspects of the materials, including structural and electronic properties, synthesis strategies, and photocatalytic mechanisms are introduced. The synergistic roles of adsorption-photocatalysis coupling, heterojunction formation, and charge carrier dynamics are insightfully discussed. Finally, perspective and outlooks for the rational design of efficient and stable BiOBr/ZSM-5 photocatalysts toward integrated environmental and energy applications are provided. This review provides guidance for the rational design of BiOBr/ZSM-5 photocatalysts toward efficient environmental remediation and sustainable hydrogen production.

Keywords: BiOBr, ZSM-5, Photodegradation, Hydrogen production, Clean energy

Introduction

Organic pollution in aquatic environments has become a critical global issue driven by intensified industrial activities, rapid urbanization, and continuous population growth [1]. Persistent contaminants such as synthetic dyes, pesticides, and pharmaceutical residues are difficult to degrade naturally and can exert long-term toxic and bioaccumulative effects on ecosystems and human health [2,3]. Conventional wastewater treatment technologies, including physical adsorption and biological processes, often demonstrate limited effectiveness toward these chemically stable pollutants [4,5]. In many cases, these methods merely transfer contaminants from one phase to another without achieving complete mineralization [6]. Consequently, there is an urgent need for advanced treatment strategies capable of not only removing organic pollutants but also converting them into environmentally benign products [7].

In parallel with environmental challenges, the global energy crisis associated with fossil fuel depletion and increasing carbon emissions has intensified the search for sustainable and clean energy alternatives [8]. Hydrogen has emerged as a promising energy carrier due to its high energy density and the absence of carbon emissions during utilization [9]. However, the large-scale production of hydrogen using environmentally friendly methods remains a significant challenge [10]. Solar driven technologies offer a viable pathway for sustainable hydrogen generation, particularly when integrated with environmental remediation processes [11]. Therefore, developing multifunctional systems capable of simultaneously addressing water pollution and clean energy production has attracted growing research interest [12].

Semiconductor based photocatalysis has been widely investigated as an effective approach to tackle both environmental pollution and renewable energy generation [13]. By harnessing solar energy, photocatalysis can initiate redox reactions through the excitation of electrons from the valence band to the conduction band [14]. In pollutant degradation processes, photogenerated reactive oxygen species are able to oxidize complex organic molecules into simpler and less harmful substances [15,16]. Similarly, in hydrogen production, photocatalysis enables water splitting through the hydrogen evolution reaction driven by high energy electrons [17]. Despite these advantages, the practical application of photocatalysis is still hindered by issues such as rapid electron hole recombination, limited visible light utilization, and insufficient long-term stability of conventional photocatalysts [18].

Among various semiconductor photocatalysts, bismuth-based materials, particularly bismuth oxybromide (BiOBr), have attracted increasing attention in recent years [19]. BiOBr features a unique layered structure composed of alternating $[Bi_2O_2]^{2+}$ and Br^- layers, which generates an internal electric field that promotes efficient charge separation [20]. Its bandgap is well suited for visible light activation, making BiOBr highly attractive for solar driven photocatalytic applications [21]. Numerous studies have demonstrated that BiOBr exhibits superior photocatalytic performance under visible light compared with traditional TiO_2 based photocatalysts [22]. Nevertheless, the photocatalytic efficiency of pristine BiOBr is still limited by its relatively low surface area, restricted number of active sites, and residual electron hole recombination [23]. To address these limitations, the construction of composite photocatalysts by integrating BiOBr with porous supporting materials has emerged as a promising strategy. Zeolite ZSM-5 is particularly attractive due to its well-defined microporous framework, high surface area, and excellent thermal and chemical stability [24,25]. The strong adsorption capability of ZSM-5 toward organic molecules can increase the local concentration of pollutants near photocatalyticaly active sites [26,27]. Moreover, ZSM-5 can regulate reactant diffusion and enhance the dispersion of BiOBr, leading to improved exposure of active facets. The interaction between BiOBr and ZSM-5 is also expected to facilitate interfacial charge transfer and suppress electron hole recombination, thereby enhancing overall photocatalytic performance in **Figure 1**.

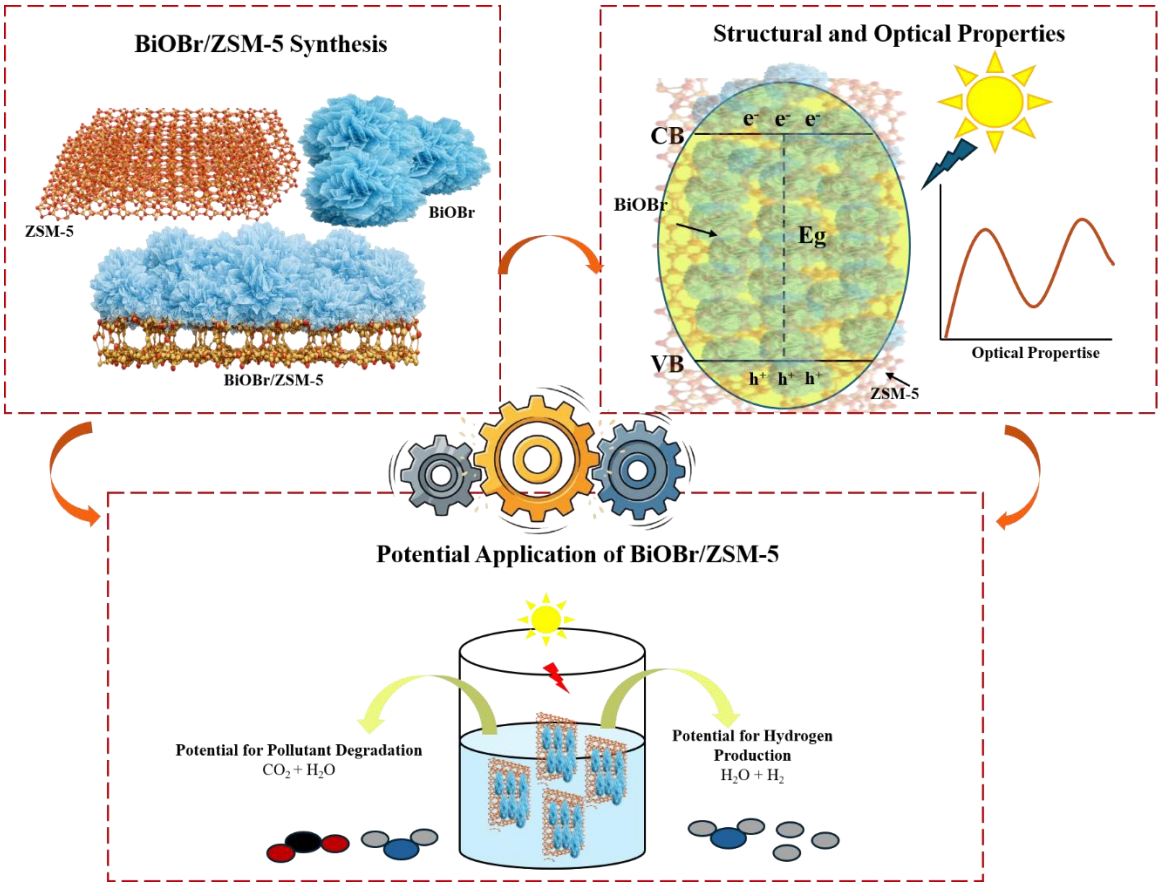


Figure 1 Schematic illustration of BiOBr/ZSM-5 composite photocatalysts for pollutant degradation and hydrogen production under visible-light irradiation. The incorporation of ZSM-5 into the BiOBr-based photocatalyst facilitates the interaction between the photocatalyst and target pollutants while contributing to the separation of photogenerated charge carriers. Under visible-light irradiation, the generated electrons and holes participate in photocatalytic reactions, enabling pollutant degradation and/or hydrogen production.

Despite the substantial progress achieved in the development of BiOBr-based photocatalysts, several research gaps remain regarding their integration with porous support materials, particularly ZSM-5. Numerous studies have reported the development of BiOBr-based composites with various semiconductors and functional materials, demonstrating the promising photocatalytic performance of BiOBr for environmental applications, particularly in the degradation of organic pollutants. However, despite these promising photocatalytic properties, the application of BiOBr-based materials for photocatalytic hydrogen production remains relatively limited, indicating that the potential of BiOBr for solar-driven hydrogen evolution has not yet been fully explored. In parallel, ZSM-5 has been widely employed as a supporting material in photocatalytic systems due to its well-defined porous structure, adsorption capability, and chemical stability. Nevertheless, the specific application of ZSM-5 as a support for BiOBr-based photocatalysts remains rarely investigated. Consequently, the combination of BiOBr and ZSM-5 represents an emerging research area that warrants further exploration, particularly for photocatalytic hydrogen production, where the photocatalytic properties of BiOBr could potentially be complemented by the porous and adsorptive characteristics of ZSM-5. Moreover, although several studies have investigated BiOBr-based composites, comprehensive reviews specifically focusing on the integration of BiOBr with ZSM-5 remain limited. Therefore, this review provides a comprehensive and critical overview of recent advances in BiOBr/ZSM-5 photocatalysts, with particular emphasis on their synthesis strategies, structure–property–performance relationships, photocatalytic mechanisms, and applications in environmental remediation and

hydrogen production. By critically evaluating the current state of research, this review highlights the limited exploration of BiOBr/ZSM-5 systems for photocatalytic hydrogen production and identifies key research opportunities for further investigation. Finally, current challenges and future perspectives are discussed to provide guidance for the rational design of efficient and sustainable BiOBr/ZSM-5 photocatalytic systems for integrated environmental and energy applications.

Fundamental of BiOBr for photocatalytic applications

Structural and electronic properties of BiOBr

BiOBr is an important member of the bismuth oxyhalide family (BiOX, X = Cl, Br, I) and is characterized by a distinctive layered crystal structure with tetragonal symmetry [28]. This structure consists of positively charged $[Bi_2O_2]^{2+}$ slabs alternately stacked with bromide (Br^-) ion layers, forming an anisotropic arrangement along specific crystallographic direction [29]. Such a layered architecture is a defining feature of BiOBr and strongly influences its physicochemical behavior. The alternating charged layers induce an intrinsic internal electric field within the crystal lattice. This built-in electric field plays a crucial role in facilitating the separation of photogenerated charge carriers. As a result, electron hole recombination is suppressed, leading to improved photocatalytic efficiency under light irradiation [30].

BiOBr exhibits a band gap in the range of approximately 2.7 - 2.9 eV, enabling its activation under visible-light irradiation [29,31]. The valence band (VB) of BiOBr is mainly composed of O 2p and Br 4p orbitals, while the conduction band (CB) is dominated by Bi 6p orbitals. The significant contribution of Br 4p orbitals raises the valence band position relative to that of many conventional oxide semiconductors, endowing BiOBr with strong oxidation capability. This electronic configuration is advantageous for driving oxidative photocatalytic reactions. Moreover, the presence of 2 valence bands with different energy levels has been reported to provide enhanced redox flexibility. This feature enables BiOBr to simultaneously support oxidation of organic pollutants and reduction reactions, including hydrogen evolution, within a single photocatalytic system [32,33].

Despite these favorable structural and optoelectronic properties, pristine BiOBr still faces several limitations in practical applications. The recombination rate of photogenerated charge carriers remains relatively high, which restricts overall photocatalytic efficiency. In addition, the intrinsically limited active surface area of bulk BiOBr reduces the number of accessible reactive sites. BiOBr particles also tend to agglomerate during synthesis or operation, further decreasing effective surface exposure. These factors collectively hinder optimal utilization of photogenerated electrons and holes in catalytic reactions. Consequently, the development of effective strategies to enhance charge separation and maximize surface activity has become a critical focus in the rational design of BiOBr-based photocatalytic materials [34].

Synthesis of BiOBr

BiOBr possesses a suitable band gap energy and features 2 distinct valence bands (VBs) with different oxidation capabilities, in which one valence band responds primarily to ultraviolet light while the other is active under visible-light irradiation. This unique electronic band structure and favorable band alignment enable BiOBr to exhibit excellent photocatalytic oxidation and reduction performance when exposed to a broad light spectrum [35]. As a result, BiOBr has been extensively applied for the degradation of various environmental contaminants, including dyes, phenolic compounds, bacteria, toluene, and persistent organic pollutants such as tetrabromobisphenol A [36,37]. The photocatalytic performance of BiOBr is strongly influenced by its crystal structure and morphology, which directly affect light absorption, charge transport, and surface reactivity. Consequently, a wide range of synthesis strategies has been developed to tailor these properties and optimize the photocatalytic activity of BiOBr [38].

Hydrothermal method is one of the most widely employed techniques for synthesizing BiOBr with controlled morphology. Siao *et al.* [39] reported that hydrothermal synthesis of BiOBr with pH regulation using NaOH resulted in flower-like microstructures. Similar observations were reported by Jia *et al.* [40] who successfully synthesized flower-like BiOBr at pH 1, while higher pH values induced significant

morphological transformations. Lu *et al.* [41] further investigated the effect of pH values (1, 3, 5 and 7) on the structure of BiOBr for bisphenol A degradation. The results demonstrated that increasing pH led to reduced crystallite size and nanosheet thickness, accompanied by an increase in specific surface area. These structural modifications directly contributed to enhanced photocatalytic activity, highlighting the critical role of pH control during hydrothermal synthesis.

In addition to pH effects, crystal facet engineering plays a crucial role in governing charge transport dynamics and photocatalytic activity of BiOBr. Modifications of the $[Bi_2O_2]$ layers and halogen atom arrangements can expose different crystal facets, such as (001) and (010), which exhibit distinct photocatalytic reactivities [40]. It has been reported that the efficiency of gas-phase Hg^0 oxidation over BiOBr is strongly dependent on synthesis pH conditions, with photocatalytic efficiencies of 54%, 60%, 65%, and 61% observed at pH values of 2, 7, 10, and 13, respectively. These results confirm that pH regulation during synthesis can effectively control the exposure of active crystal facets. Consequently, facet engineering emerges as a powerful strategy for enhancing the photocatalytic performance of BiOBr [40].

The influence of BiOBr morphology has also been extensively studied in photoelectrochemical (PEC) applications. Zhang *et al.* [42] reported the hydrothermal synthesis of flower-like BiOBr with a large surface area using ethylene glycol as a solvent, which exhibited the highest photocurrent response for chloramphenicol detection. Furthermore, Sun *et al.* [43] investigated the PEC performance of BiOBr thin films synthesized via chemical vapor deposition using a mixed solvent system of DMF and HNO_3. The resulting BiOBr films displayed the highest photocurrent density, which was attributed to their continuous surface morphology and moderate thickness. These structural features were found to effectively promote charge separation and electron hole transport, thereby enhancing PEC performance.

The solvothermal method has also been widely used to produce various BiOBr morphologies, including microflowers, microspheres, and nanosheets, particularly for gas-phase pollutant degradation under visible light. BiOBr microflowers exhibited the highest specific surface area and superior photocatalytic activity compared to other morphologies. This enhanced performance was associated with the dominant exposure of the (001) facet and the formation of surface oxygen vacancies. The presence of oxygen vacancies contributed to bandgap narrowing by shifting the positions of the valence and conduction bands, thereby improving light absorption and electron trapping capability [43]. Additionally, BiOBr syntesized by solvothermal method could control the morphology by modifying the seolvent and the use of surfactant [44,45].

Overall, numerous studies indicate that hydrothermal and solvothermal methods are the primary approaches for synthesizing BiOBr with nanosheet and microspherical morphologies. Variations in pH, solvent type, and surfactant concentration exert direct influence on particle size, specific surface area, and exposure of active crystal facets, which collectively determine the photocatalytic performance of BiOBr as presented in **Table 1**. While the photocatalytic efficiency of BiOBr for pollutant degradation has been widely reported, further research is still required to fully explore its potential in hydrogen production, antibacterial applications, and sensor systems.

Table 1 List of reported BiOBr with different synthesis methods and morphologies for various catalytic process carried out under visible light irradiation.

No.	Material	Synthesis Method	Starting Material	Solvent used	Morphology	Result	Ref
1	BiOBr	Co-precipitation	$Bi(NO_3)_3.5H_2O$, Kbr, absolute ethanol, EG, NaOH	Deionised water	Nanoflowers self-assembled from nanosheet	Oxidation of Hg, BiOBr-2, BiOBr-7, BiOBr-10, BiOBr-13; 54%, 60%, 65%, and 61%	[40]
2	BiOBr	Chemical vapor deposition	$BiBr_3$	DMF, HNO_3	Nanoplates	-	[43]
3	BiOBr	Hydrotermal	$BiBr_3$	Deionised water	Flower-like	Crystal violet	[46]

No.	Material	Synthesis Method	Starting Material	Solvent used	Morphology	Result	Ref
4	BiOBr	Hydrotermal	$BiBr_3$, NaOH	Desionised water	Irregular sheet	Crystal violet	[47]
5	BiOBr	Hydrotermal	$Bi(NO_3)_3.5H_2O$, Hexadecyl Trimethyl Ammonium Bromide (HTAB)	EG	Flower-like	Detection of chloramphenicol	[42]
6	BiOBr	Hydrotermal	$Bi(NO_3)_3.5H_2O$, KBr, HNO_3 NaOH	Deionised water	Flower-like	Crystal violet	[48], [49]
7	BiOBr	Hydrotermal	$Bi(NO_3)_3.5H_2O$, KBr, HNO_3, NaBr NaOH	Deionised water	pH 7, Flower-like microstructure	Highest BPA degradation performance (pH 7) within 120 min	[41]
8	BiOBr	Solvothermal	$Bi(NO_3)_3.5H_2O$, KBr, absolute ethanol, EG	Absolute ethanol, EG, distilled water	Microflower,	o-DCB, NT, MS, and MF 51%, 59%, 68%, 6h	[50], [51]
9	BiOBr	Solvothermal	$Bi(NO_3)_3.5H_2O$, KBr, absolute ethanol, EG, acetic acid, NaBr, CH_3OH, n-butanol, n-5-hexanol, n-hexyl acetate	Methanol	Nanosheet	RhB, 100%, 32 min	[52]
10	BiOBr	Solvothermal	$Bi(NO_3)_3.5H_2O$, KBr,	EG, Isopropanol, CTAB surfactan	Flower-like microspheres	RhB, 95%, 50 min	[22]

BiOBr composites

Previous study reported that Bi_2O_4/BiOBr nanosheets synthesized via a base-induced hydrothermal method exhibited significantly higher photocatalytic reaction rates compared to pristine BiOBr [53,54]. This enhanced performance was attributed to the incorporation of the Bi_2O_4 phase, which broadened visible-light absorption, promoted the separation of photogenerated electron–hole pairs, and improved the adsorption of reactants on the catalyst surface. Bi_2O_4 nanoparticles were formed on the surface of BiOBr nanosheets through NaOH-induced dehalogenation and oxidation by photogenerated holes (h^+). Furthermore, the amount of the Bi_2O_4 phase could be readily tuned by adjusting the NaOH concentration during post-synthesis treatment while preserving the highly reactive (001) facet of BiOBr. In addition to the degradation of organic pollutants, Bi_2O_4/BiOBr heterostructures have also shown considerable potential for photocatalytic CO_2 reduction. Bi_2O_4/BiOBr nanosheets treated with 0.01 M NaOH exhibited substantially enhanced activity for converting CO_2 into CO and CH_4 under simulated solar irradiation, whereas pristine BiOBr displayed negligible photocatalytic performance. This remarkable improvement was attributed to the enhanced separation and migration of photogenerated charge carriers resulting from the formation of the Bi_2O_4/BiOBr heterojunction. These findings suggest that heterojunction engineering not only improves pollutant degradation but also broadens the application of BiOBr-based photocatalysts toward solar fuel production [55].

Similarly, the construction of more complex heterojunctions has been reported to further improve photocatalytic efficiency. Ternary m-Bi_2O_4/Bi_2O_{4-x}/BiOCl heterojunction was successfully synthesized via a hydrothermal method by regulating the amount of concentrated HCl during the synthesis process. The resulting architecture consisted of BiOCl nanosheets

serving as the supporting matrix, onto which m-Bi_2O_4 microrods and Bi_2O_{4-x} nanospheres were uniformly anchored. Under visible-light irradiation, the photocatalyst achieved degradation efficiencies of 98.3% for bisphenol A (BPA) within 30 min and 82.3% for ciprofloxacin (CIP) within 80 min. The corresponding reaction rate constants were approximately 30.16 and 2.82 times higher than those of pristine BiOCl, respectively. The superior performance was attributed to the synergistic charge-transfer pathways involving both type-II heterojunction and direct Z-scheme mechanisms, which promoted efficient separation and migration of photogenerated electron–hole pairs while suppressing charge recombination. Photoluminescence (PL) and photoelectrochemical (PEC) analyses further confirmed enhanced charge-transfer efficiency and successful heterojunction formation. In addition, the photocatalyst exhibited excellent stability, retaining approximately 90% of its initial photocatalytic activity after 4 consecutive degradation cycles [56]. Collectively, these studies demonstrate that rational heterojunction engineering, including binary Bi_2O_4/BiOBr and ternary m-Bi_2O_4/Bi_2O_{4-x}/BiOCl systems, is an effective approach for improving the visible-light response, charge-carrier separation, and photocatalytic performance of bismuth-based photocatalysts. Furthermore, the successful application of these heterostructures in both organic pollutant degradation and CO_2 photoreduction highlights their potential for broader environmental remediation and solar energy conversion applications [56].

$PbBiO_2Br$/BiOBr heterostructures was synthesized via a hydrothermal method with pH values varied from 1 to 14 using NaOH. The pH adjustment resulted in diverse morphologies, including square plates, flower-like architectures, rod-like structures, and irregular nanosheets. These structural variations had a pronounced impact on the optoelectronic properties of the materials, leading to a reduction in bandgap energy from 2.80 to 2.42 eV. Photocatalytic performance evaluation using crystal violet (CV) dye demonstrated a significant enhancement in activity. This improvement was primarily attributed to the formation of an effective $PbBiO_2Br$/BiOBr heterojunction, which facilitated the separation and migration of photoinduced charge carriers [46,57].

Similar findings have also been reported in other studies involving BiOBr-based composites with different bismuth-containing compounds. Liu *et al.* [58] synthesized BiOAc/BiOBr composites via a hydrothermal route for the degradation of Rhodamine B (RhB). The results revealed that coupling BiOAc with BiOBr effectively narrowed the bandgap energy from 3.31 to 2.64 eV. As a consequence, the RhB degradation efficiency increased dramatically from 70% for pristine BiOBr to 98% for the BiOAc/BiOBr composite [58]. Overall, these studies demonstrate that BiOBr based composites developed through heterostructure engineering consistently exhibit enhanced photocatalytic performance under solar light irradiation, as summerized in **Table 2**.

Table 2 Performance of BiOBr-based material for photocatalytic degradation studied under solar light illumination.

Material	Synthesis method	Starting materials	Solvent used	Band gap energy (eV)	Photocatalytic degradation efficiency %	Ref
Bi_2O_4/BiOBr	Alkali induced/ hydrothermalCo-precipitation	$Bi(NO_3)_3{\cdot}5H_2O$, KBr, NaOH	Distilled water	2.8	MO, BiOBr - 55%, 30 min Bi_2O_4/BiOBr - 100%, 10 min	[53,54]
Black phosphorus nanosheets/BiOBr (BPN–Bi)	Co-precipitation	Red phoshorus, $Bi(NO_3)_3{\cdot}5H_2O$, KBr, NaOH	Deionised water	-	BiOBr MO - 13.4% CIP - 60.5%	[59]

Material	Synthesis method	Starting materials	Solvent used	Band gap energy (eV)	Photocatalytic degradation efficiency %	Ref
					BPNs MO - 10.2%, CIP - 8.3%, 60 min 15BPN-Bi MO - 98.8% CIP - 98.2%	
Bi_2S_3/BiOBr	Co-precipitation	$Bi(NO_3)_3{\cdot}5H_2O$, CTAB, thiourea, HNO_3, methanol	HNO_3	-	-	[60]
BiOBr/$SnWO_4$	Co-precipitation	$SnCl_2{\cdot}2H_2O$, AO, isopropanol, methanol, $Na_2WO_4.2H_2O$, PVP, $Bi(NO_3)_3{\cdot}5H_2O$, KBr	EG	$SnWO_4$- 1.43 BiOBr - 2.91 BiOBr/$SnWO_4$ - 2.90	RhB, BiOBr - 65.9% BiOBr–$SnWO_4$ –1 - (97.85%) in 60 min BG, BiOBr - 78.2% BiOBr– $SnWO_4$ - 95.5%, 88.2%, 83.73% $SnWO_4$ - 55.3%, 45 min	[61]
$PbBiO_2Br$/BiOBr	Hydrothermal	$Pb(NO)_3{\cdot}H_2O$, AO, $BiBr_3$, NaOH	Deionised water	BiOBr – 2.80 PbBiO2Br/BiOBr – 2.42	CV, 98%, 72 h	[46], [57]
BiOAc/BiOBr	Hydrothermal	$Bi(NO_3)_3{\cdot}5H_2O$, Bi_2O_3, KBr, glacial acetic acid	Ethanol, deionised water	BiOAc, BiOBr 3.31, 2.64	RhB, BiOAc/BiOBr-98%, 15 min BiOBr (~70%) CIP, 75% and 50%, 120 min	[58]
BPQDs-modified BiOBr	Hydrothermal	Black phosphorus (BP) crystals, N-methyl-2-pyrrolidone, $Bi(NO_3)_3{\cdot}5H_2O$, CTAB)	EG	BiOBr, BPQDs/ BiOBr- 2.74, 2.62, 2.58, 2.49	Methyl violet (MV) BiOBr - 65% BPQDs/BiOBr - 98.2%, 4 h TC, BiOBr - 48.9% BPQDs/BiOB - 97.5%, 5 h	[62]
BiOBr–Bi_2S_3	Ion exchange	NaOH, $K_2Cr_2O_7$, $Na_2S_2O_3{\cdot}5H_2O$, H_2SO_4, KBr, diphenylcarbazide (DPC), $Bi(NO_3)_3{\cdot}5H_2O$, Ethanol, $Cr_2(SO_4)_3{\cdot}xH_2O$	Deionised water	BiOBr, B-0.25, B-2, Bi_2S_3 2.87, 2.05, 1.75, 1.42	Cr (IV), BiOBr–Bi_2S_3 - 100%, 12 min	[63]
C60/BiOBr	Microwave Hydrothermal	$Bi(NO_3)_3{\cdot}5H_2O$, acetic acid, KBr	Acetic acid	-	RhB, C60/BiOBr - 91%, 10 min BiOBr - 59%	[64]
WO_3/BiOBr	Solvothermal	Sodium tungstate dihydrate	2-methoxyethanol, EG	WO_3 - 2.62 BiOBr - 2.75	CIP, WO_3/BiOBr - 94.7%, 120 min	[65]

Material	Synthesis method	Starting materials	Solvent used	Band gap energy (eV)	Photocatalytic degradation efficiency %	Ref
		($Na_2WO_4·2H_2O$), sodium hydrogen sulfate monohydrate ($NaHSO_4·H_2O$), CTAB), 2-methoxyethanol, Bi $(NO_3)_3·5H_2O$				
CoS/BiOBr	Two step solvothermal method	$Co(OAc)_2$ $4H_2O$, $Bi(NO_3)_3·5H_2O$, CH_4N_2S, C_2H_5OH, glacial acetic acid, CH_3COOH, KBr, $Na_3PO_4·12H_2O$	Acetic acid, deionised water	BiOBr - 2.50 CoS - 1.20	Glyphosate, BiOBr - 21.9% CoS/ BiOBr - 74.7%, 3 h	[66]

As summarized in **Table 2**, BiOBr-based photocatalysts demonstrate substantially enhanced photocatalytic performance under solar-light irradiation when coupled with appropriate semiconductors or conductive materials. However, the reported studies were carried out under different experimental conditions, including catalyst loading, initial pollutant concentration, irradiation intensity, and reaction time, which strongly influence the observed degradation efficiencies and apparent reaction rates. Nevertheless, the table clearly shows that a variety of synthesis routes can be successfully employed to construct efficient BiOBr-based photocatalysts, each offering distinct advantages depending on the intended application. For example, co-precipitation is attractive for its simplicity, low cost, and ease of scale-up, making it suitable for rapid and practical material preparation. Hydrothermal and solvothermal routes are valuable when better crystallinity, controlled morphology, and intimate interfacial contact are desired, which can support efficient charge separation. Ion-exchange and microwave-assisted hydrothermal methods are also effective for tailoring composition and accelerating synthesis, respectively, while enabling the formation of well-integrated heterostructures. In addition, the incorporation of heterojunction partners such as Bi_2O_4, BiOAc, $BPQD_5$, WO_3, C_{60}, and Bi_2S_3 broadens visible-light absorption and facilitates charge transfer, thereby improving photocatalytic activity. Overall, the results indicate that different synthesis strategies can all be suitable, depending on the targeted material characteristics, processing requirements, and application goals.

BiOBr-based materials for degradation of organic pollutant

The photocatalytic degradation mechanism of organic pollutants generally involves the photoexcitation of semiconductor materials under UV or visible light irradiation, leading to the generation of electron hole (e^-/h^+) pairs. Upon light absorption, photogenerated electrons in the conduction band react with dissolved oxygen to form superoxide radicals ($·O_2^-$), while holes in the valence band oxidize surface-adsorbed water or hydroxide ions to produce hydroxyl radicals (·OH) which are the primary reactive oxygen species responsible for the oxidation and mineralization of organic contaminants [67,68]. **Figure 2** shows the photocatalytic mechanism of degradation pollutant. Recent studies have demonstrated that material modification strategies such as metal or non-metal doping, heterojunction construction, and composite formation effectively suppress charge recombination and enhance interfacial charge transfer, thereby increasing reactive oxygen species (ROS) generation [69,70]. In heterostructure systems, internal electric fields facilitate directional electron migration, promoting sustained radical formation and improved degradation pathways. Additionally, carbon-based materials and MOF-derived photocatalysts act as electron acceptors or transport media, further prolonging charge carrier lifetimes and accelerating the

breakdown of complex organic molecules into less harmful intermediate and final mineralization products such as bismuth oxyhalides (BiOX, X = Cl, Br, and I) [71].

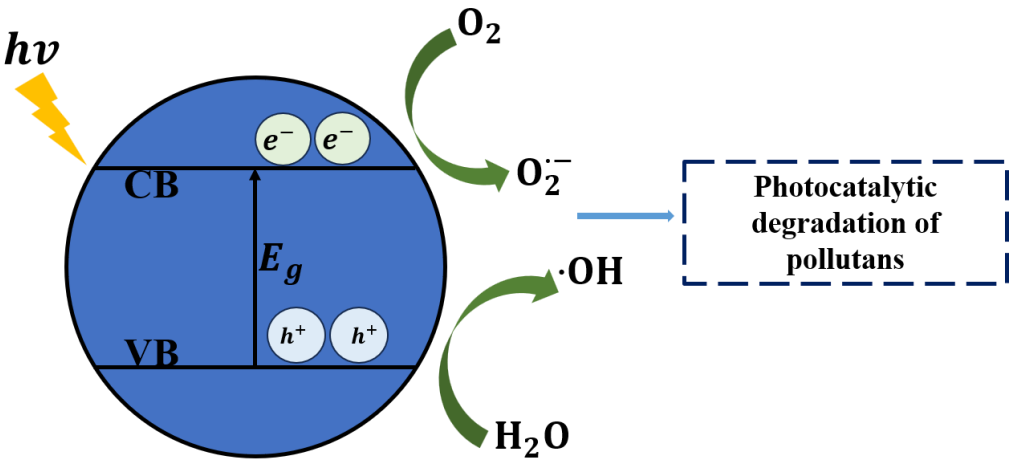


Figure 2 Schematic illustration of the photocatalytic mechanism of BiOBr for organic pollutant degradation under light irradiation. Upon irradiation, electrons are excited from the valence band (VB) to the conduction band (CB), generating photogenerated electron–hole pairs. The generated charge carriers subsequently participate in redox reactions to produce reactive species that promote the degradation of organic pollutants into less harmful products.

Various organic dyes have been extensively employed as model pollutants to evaluate the photocatalytic performance of bismuth oxyhalides (BiOX, X = Cl, Br, and I) [72]. Commonly investigated dyes include methyl orange (MO), methylene blue (MB), malachite green (MG), quinoline blue (QB), and rhodamine B (RhB), each representing different molecular structures and charge characteristics. Among these, RhB, a cationic dye, is one of the most frequently used probes due to its strong visible-light absorption and well-known photosensitization behavior. Mechanism photocatalytic degradation of bismuth oxyhalides representative in **Figure 3**.

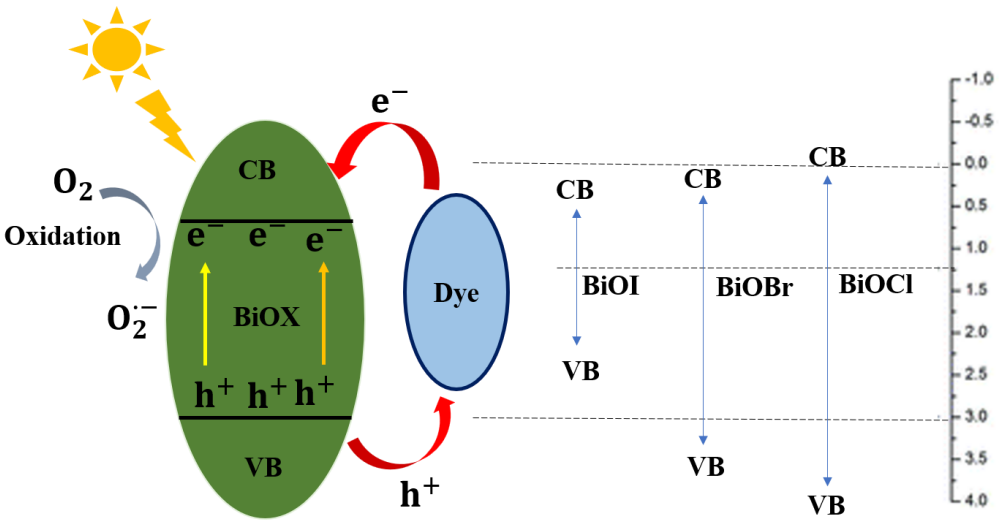


Figure 3 Schematic illustration of the photocatalytic degradation mechanism of bismuth oxyhalides (BiOX) under light irradiation. Light irradiation induces the excitation of electrons from the valence band (VB) to the conduction band (CB), resulting in the generation of photogenerated electron–hole pairs. These charge carriers interact with dye molecules through oxidation and reduction reactions, facilitating the degradation of organic pollutants into smaller and less harmful products.

Numerous studies have demonstrated the excellent capability of BiOX materials in degrading RhB. For instance, Liu *et al.* [73] reported that flower-like BiOCl synthesized via a co-precipitation method achieved complete (100%) degradation of RhB within 50 min under visible-light irradiation. SEM analysis revealed that the BiOCl consisted of 3-dimensional flower-like microspheres assembled from ultrathin nanosheets, while XRD confirmed the formation of pure tetragonal BiOCl. The hierarchical structure provided a larger surface area and more exposed active sites, whereas the increased concentration of oxygen vacancies facilitated charge separation and inhibited electron–hole recombination, resulting in enhanced photocatalytic degradation of RhB [73]. Similarly, Hao *et al.* [74] A homogeneous BiOCl/$Bi_{12}O_{17}Cl_2$ phase junction was successfully synthesized via a one-step hydrothermal method by controlling the amount of NaOH during the synthesis process. XRD analysis confirmed the coexistence of tetragonal BiOCl and $Bi_{12}O_{17}Cl_2$ phases, indicating the successful formation of the phase junction, while UV–Vis diffuse reflectance spectroscopy (DRS) revealed that the incorporation of $Bi_{12}O_{17}Cl_2$ extended the light absorption range from the UV region into the visible-light region, thereby enhancing solar energy utilization. The BiOCl/ $Bi_{12}O_{17}Cl_2$ composite exhibited significantly higher photocatalytic activity than pristine BiOCl and $Bi_{12}O_{17}Cl_2$ for the degradation of methyl orange (MO) under simulated solar irradiation and demonstrated excellent oxidation performance toward various organic pollutants, including 2,4-dichlorophenol (2,4-DCP), phenol, bisphenol A (BPA), and tetracycline hydrochloride. Photoluminescence (PL) and photoelectrochemical analyses further revealed a lower electron–hole recombination rate and more efficient charge transfer in the composite compared with the individual components. The enhanced photocatalytic performance was attributed to the formation of a BiOCl/ $Bi_{12}O_{17}Cl_2$ phase-junction interface, which promoted the separation of photogenerated electron–hole pairs, facilitated charge migration to the catalyst surface, and increased the generation of reactive species, resulting in superior photocatalytic activity toward a broad range of organic contaminants [74].

Ao *et al.* [75] developed a novel p–n heterojunction photocatalyst by integrating BiOCl nanoparticles onto titanium phosphate (TP) nanoplates through an in-situ growth process. Structural characterization by XRD confirmed the successful coexistence of BiOCl and TP phases without the formation of secondary impurities, while SEM and TEM analyses revealed that BiOCl particles were uniformly anchored on the surface of the TP nanoplates, establishing intimate interfacial contact between the 2 semiconductors. UV–Vis DRS results further demonstrated enhanced light-harvesting capability after BiOCl incorporation. Owing to the formation of the p–n heterojunction, the BiOCl/TP composite exhibited remarkably improved photocatalytic performance toward the degradation of a wide range of organic pollutants, including Rhodamine B (RhB), methylene blue (MB), Reactive Brilliant Red X-3B (X-3B), ciprofloxacin, and phenol. Photoelectrochemical and photoluminescence analyses indicated more efficient charge separation and reduced electron–hole recombination in the composite system. The superior photocatalytic activity was attributed to the built-in electric field formed at the BiOCl/TP interface, which facilitated interfacial charge transfer and promoted the generation of reactive species responsible for pollutant degradation [75].

Reasearch by Phuruangrat *et al.* [76] synthesized BiOI nanoplates via a simple sonochemical method and investigated the effect of precursor solution pH on the phase composition, morphology, and photocatalytic performance of the material. XRD, TEM, SAED, and XPS analyses confirmed the formation of pure tetragonal BiOI nanoplates at pH values ranging from 8 to 12. The photocatalytic activity was evaluated through the degradation of Rhodamine B under visible-light irradiation, revealing that the sample synthesized at pH 12 exhibited the highest degradation efficiency of 81.19% after 180 min. The enhanced performance was attributed to the improved crystallinity, phase purity, and well-defined nanoplate morphology, which provided more active sites for photocatalytic reactions [76].

Among the various synthesis approaches, the solvothermal method has attracted considerable attention due to its ability to provide precise control over

crystal growth, morphology, phase composition, and interfacial structure under relatively mild reaction conditions. This method is particularly effective for constructing semiconductor heterojunctions with intimate interfacial contact, which is crucial for enhancing charge separation and photocatalytic performance. Using this approach, Cai *et al.* [51] synthesized BiOI/BiOBr heterojunctions through an ionic liquid-assisted one-pot solvothermal process. XRD, SEM, and HRTEM analyses confirmed the successful formation of a tightly coupled heterojunction structure composed of BiOI and thin BiOBr nanosheets. Furthermore, BET measurements revealed that the heterojunction exhibited a specific surface area of 11.6 m^2/g, providing more accessible active sites for photocatalytic reactions. As a result, the BiOI/BiOBr heterojunction exhibited significantly enhanced photocatalytic activity toward RhB degradation under simulated sunlight irradiation. The improved performance was attributed to the synergistic effects of increased surface hydroxyl groups, enlarged surface area, and efficient separation and migration of photogenerated charge carriers across the heterojunction interface, which effectively suppressed electron–hole recombination. Reasearch by Huo *et al.* [77] synthesized hierarchical flower-like BiOBr microspheres via a solvothermal method and reported nearly complete RhB degradation 95% within 60 min under visible-light irradiation. XRD analysis confirmed the formation of highly crystalline tetragonal BiOBr, while SEM observations revealed a 3-dimensional flower-like architecture assembled from nanosheets. The superior photocatalytic performance was attributed to the enhanced visible-light harvesting arising from multiple light reflections within the hierarchical structure, efficient separation of photogenerated charge carriers, high crystallinity, and large surface area. Furthermore, trapping experiments identified superoxide radicals ($\cdot O_2^-$) as the dominant reactive species during the photocatalytic degradation process [77].

Morphological engineering has been widely recognized as an effective strategy for enhancing the photocatalytic performance of BiOI-based materials, as hierarchical architectures can provide abundant active sites, improved light harvesting, and enhanced charge transport. In this context, Long *et al.* [78] successfully synthesized porous hierarchical BiOI nanostructures at room temperature without the use of surfactants. Structural and morphological characterizations, including XRD, XPS, FESEM, TEM, and nitrogen adsorption–desorption analyses, confirmed the formation of hierarchical architectures assembled from interconnected nanosheets with a relatively high specific surface area of 64.5 m^2 /g. Photocatalytic experiments demonstrated that the synthesized BiOI achieved degradation efficiencies of 98.7%, 43.2%, and 76.9% for Rhodamine B (RhB), methylene blue (MB), and methyl orange (MO), respectively, after 180 min of visible-light irradiation. In addition to its excellent photocatalytic activity, the material exhibited remarkable antibacterial performance against *Bacillus* sp. and *Pseudoalteromonas* sp. Mechanistic studies revealed that superoxide radicals ($\cdot O_2^-$) and photogenerated holes (h^+) were the dominant reactive species involved in pollutant degradation. The enhanced performance was attributed to the synergistic effects of the large specific surface area, negatively charged surface, and intrinsic electronic structure of BiOI, which collectively facilitated pollutant adsorption and charge transfer processes [78].

In contrast, methyl orange (MO), an anionic dye, exhibits more varied degradation behavior depending on the halide component and synthesis conditions of BiOX. Research conducted by Chen *et al.* [80] showed that the BiOCl-(001)/AgBr composite synthesized through the in-situ attachment method has very high photocatalytic activity under LED irradiation. The test results showed that the material was able to degrade approximately ~99% of methyl orange (MO) and ~95% - 98% of Rhodamine B (RhB). This increased activity is associated with the formation of a heterojunction between BiOCl and AgBr which allows for more efficient separation and transfer of photogenerated charges, thereby suppressing electron–hole recombination and increasing the formation of reactive species that play a role in the pollutant degradation process [79]. Previous study Li *et al.* [59] reported that pure BiOBr achieved 55% MO degradation within 30 min, whereas obtained a much lower degradation efficiency of only 13.4% within 1 h under different synthesis conditions. Notably, BiOI appears to outperform BiOCl and BiOBr in MO degradation [59]. Research by Li *et al.* [81] reported that iodine-deficient BiOI nanosheets has the potential to Photocatalytic tests

demonstrated significantly enhanced performance compared to pristine BiOI, achieving approximately 95–98% degradation of Rhodamine B under visible-light irradiation within the reaction time [80]. These findings suggest that BiOI possesses a more favorable band structure and surface interaction for degrading anionic dyes.

Methylene blue (MB), another widely used cationic dye, generally shows lower degradation efficiencies over BiOX photocatalysts compared to RhB. Based on the results of research conducted by Zhang *et al.* [81], the results of the photodegradation test of methylene blue (MB) showed significant differences in performance in each material. Pure BiOCl has a relatively low photocatalytic activity with a degradation rate of around 50% - 60%, which is related to limitations in light absorption and high recombination of electron–hole pairs. Pure $AgVO_3$ shows improved performance with a degradation efficiency of around 65% - 75%, indicating a better ability to respond to visible light. In the Ag/BiOCl binary system, the degradation efficiency increases further to around 80% - 85% due to increased charge separation and the contribution of Ag in accelerating the formation of reactive species. The highest performance was obtained in the ternary $Ag/AgVO_3$/BiOCl composite with a degradation efficiency of around 95% - 99%, indicating that almost all MB molecules were successfully degraded within a certain irradiation time (±60 - 120 min). This increase indicates a synergistic effect between the 3 components resulting in more effective charge separation, increased visible light absorption, and the formation of more dominant active oxidative species in the photodegradation process [81]. A similar study was also conducted by Pan *et al.* [82], who reported that the modification of BiOCl through the incorporation of rosemary powder effectively increased the concentration of oxygen vacancies and improved visible-light absorption, thereby significantly enhancing the photocatalytic activity compared to pristine BiOCl. The photodegradation results for dye removal (commonly methylene blue or other model dyes) showed that pristine BiOCl achieved only approximately 50% - 60% degradation, whereas the BiOCl–rosemary powder composite exhibited a markedly improved efficiency of around 85% - 90% under visible-light irradiation within a given reaction time. This enhancement is attributed to the role of rosemary powder in facilitating the formation of oxygen vacancies, which in turn promotes more efficient electron–hole separation and increases the generation of reactive species such as $\cdot OH$ and $\cdot O_2^-$, both of which play a crucial role in the degradation process [82]. Overall, the relatively low photodegradation performance of BiOX toward MB suggests that adsorption behavior, surface charge properties, and dye catalyst interactions play a critical role beyond intrinsic photocatalytic activity.

Based on these studies, several general trends can be identified. All BiOX materials exhibit excellent performance in degrading RhB, largely due to strong adsorption and photosensitization effects. BiOI tends to show superior performance for MO degradation compared to BiOCl and BiOBr, whereas the degradation of MB remains comparatively limited across all BiOX systems. These variations can be attributed to differences in dye charge, molecular structure, and surface interactions with the photocatalyst. The surface charge of BiOX, which is strongly influenced by solution pH, determines the adsorption affinity toward cationic or anionic dyes, while the Brunauer Emmett Teller (BET) surface area directly affects the number of accessible active sites.

Morphology and synthesis methods play a crucial role in governing photocatalytic performance. Different preparation routes result in distinct morphologies, such as nanosheets, microflowers, or hierarchical structures, which in turn regulate specific surface area, light harvesting capability, and charge carrier mobility. Changes in pH during synthesis can further alter morphology, thereby influencing adsorption behavior and photocatalytic reaction rates. From a mechanistic perspective, several studies have highlighted the role of photosensitization in RhB degradation over BiOCl. It has been reported that the unique microflower structure of BiOCl facilitates the excitation of RhB molecules, where electrons from the highest occupied molecular orbital (HOMO) of RhB are promoted to the lowest unoccupied molecular orbital (LUMO) under light irradiation. These photoinduced electrons can then be injected into the conduction band (CB) of BiOCl, subsequently reacting with dissolved oxygen to generate superoxide radicals (O_2^+), which directly participate in RhB decomposition [84]. This photosensitization

mechanism is schematically illustrated in **Figure 3**. Furthermore, the valence band position of BiOCl microflowers has been reported to be as high as +3.32 eV, exceeding the oxidation potential of $OH^-/\cdot OH$ (+2.38 eV), indicating that hydroxyl radicals (·OH) are predominantly generated through hole driven oxidation processes. Reaseach by Intaphong *et al.* [76] reported that BiOI nanoplates were successfully synthesized via a sonochemical method, producing a layered structure with thin plate-like morphology. This structure provides a higher specific surface area and enhances the efficiency of electron–hole separation. The material exhibits a narrow band gap of approximately 1.7 - 1.9 eV, enabling effective absorption of visible light and making it highly active as a visible-light-driven photocatalyst. Photodegradation tests of dye pollutants demonstrated that BiOI nanoplates achieved a high degradation efficiency of approximately ±85 - 95% within 60 - 120 min of irradiation, depending on experimental conditions such as initial concentration and light intensity. This excellent performance is attributed to the effective generation of electron–hole pairs, which subsequently produce reactive species such as $\cdot O_2^-$ and ·OH. These reactive oxygen species play a crucial role in oxidizing and decomposing dye molecules, confirming the strong potential of BiOI nanoplates as an efficient visible light photocatalyst [76].

BiOBr-based Materials for Hydrogen Evolution Potential

Hydrogen has emerged as a highly promising energy vector for future energy systems. Hydrogen possesses a high gravimetric energy density and produces only water as a by-product when utilized in fuel cells or combustion processes, thereby offering a carbon-free energy pathway compared to conventional fossil fuels that generate CO_2 and other harmful pollutants [84]. These advantages position hydrogen as a key component in global decarbonization strategies, particularly in sectors that are difficult to electrify, such as heavy industry and long-distance transportation. As illustrated in **Figure 4**, hydrogen can be produced from various energy sources, including renewables, fossil fuels, and nuclear energy, and can subsequently be utilized in multiple sectors such as power generation, transportation, chemical industries, pharmaceutical applications, synthetic fuel production, and ammonia fertilizer manufacturing.

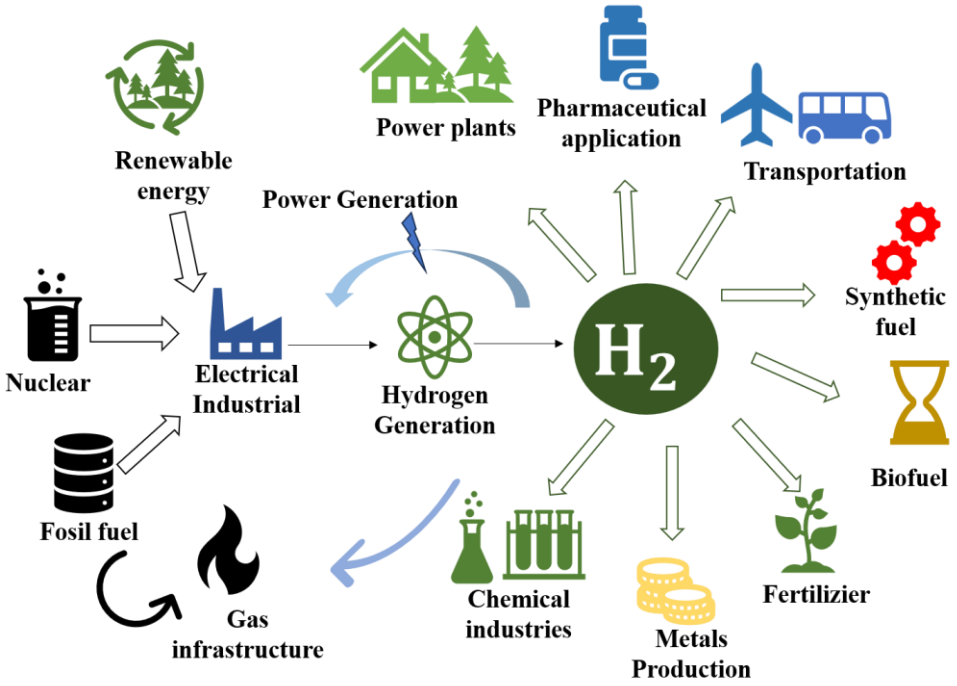


Figure 4 Schematic illustration of hydrogen production routes and their diverse end-use applications. Hydrogen can be produced from renewable and conventional energy sources and serves as a clean energy carrier for transportation, industrial processes, power generation, energy storage, and residential applications.

Photocatalysis for hydrogen production has emerged as one of the most promising renewable energy technologies due to its ability to directly utilize solar energy to drive water splitting into hydrogen and oxygen. In this process, semiconductor photocatalysts absorb incident light, generating photoexcited electrons and holes that subsequently participate in redox reactions on the catalyst surface [84]. Compared with conventional hydrogen production routes such as water electrolysis and natural gas reforming, photocatalysis offers superior environmental compatibility, as it relies primarily on sunlight as a clean and inexhaustible energy source and avoids direct carbon emissions. Nevertheless, the practical implementation of photocatalytic hydrogen production remains challenging, particularly in terms of achieving high quantum efficiency, long term stability, and cost-effective material synthesis [85].

Previous studies have demonstrated that BiOBr based photocatalysts can effectively enhance hydrogen evolution performance, especially when combined with strategies such as heterojunction construction, elemental doping, or cocatalyst loading to improve charge separation and surface reaction kinetics. Study by Hussaein *et al.* [86] reported that the optimized system, BiOX combined in a heterojunction structure showed a significantly higher hydrogen evolution activity compared to the original material, because the electrons generated from light excitation can be more effectively used to reduce protons to H_2 on the catalyst surface [86]. This finding is further supported by the study conducted by Wang *et al.* [87], who demonstrated highly efficient photocatalytic performance for simultaneous hydrogen production and antibiotic degradation under visible-light irradiation. The photocatalyst consists of g-C_3N_4, BiOBr, and α-Fe_2O_3, each playing a crucial role in the ternary Z-scheme mechanism. g-C_3N_4 acts as the primary electron donor with a strong reduction potential, enabling efficient hydrogen evolution from protons (H^+), while BiOBr serves as a charge-transfer mediator that facilitates interfacial electron migration and enhances electron–hole separation between the semiconductors. Meanwhile, α-Fe_2O_3 functions as a strong oxidation center, providing photogenerated holes (h^+) that drive water oxidation and antibiotic degradation. The results show that the optimal sample (5.2% FBC) achieves a hydrogen evolution rate of 2.57 mmol g^{-1} h^{-1}, accompanied by approximately 94% degradation of ciprofloxacin within 2 h, whereas another composition (2.4% FBC) exhibits a hydrogen production rate of 1.86 mmol g^{-1} h^{-1} with around 90% degradation of levofloxacin in the same time period. This enhanced performance is attributed to the formation of a ternary Z-scheme heterojunction, which efficiently promotes charge separation, preserves strong redox potentials, and optimizes the utilization of photogenerated electrons for hydrogen evolution and holes for pollutant oxidation, resulting in superior and stable photocatalytic activity [87].

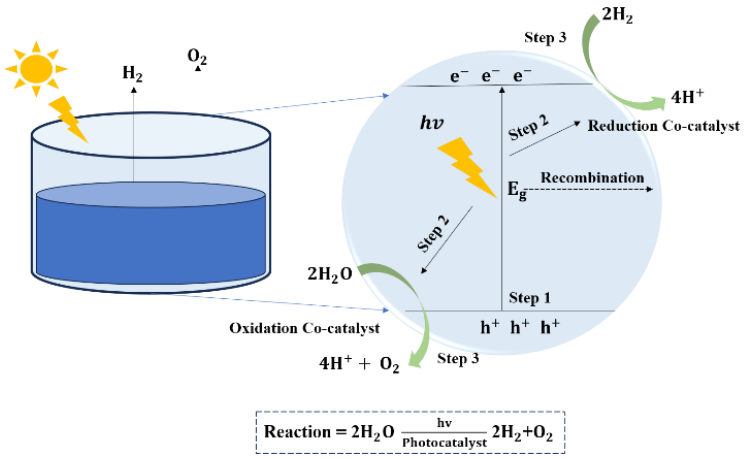


Figure 5 Schematic illustration of the basic principle of photocatalytic water splitting over a semiconductor photocatalyst. Upon light irradiation with energy equal to or greater than the band gap (*E*g), electrons are excited to the conduction band, leaving holes in the valence band, where the separated charge carriers drive reduction and oxidation reactions for hydrogen production

The fundamental mechanism of photocatalytic water splitting over semiconductor materials is illustrated in **Figure 5**. In a particulate photocatalytic system, the reaction proceeds through 3 main stages. First, photons with energy (hν) equal to or greater than the band gap energy (Eg) of the semiconductor are absorbed by the photocatalyst surface, resulting in the excitation of electrons from the VB to the CB. This excitation generates photogenerated electrons in the CB and corresponding holes in the VB, rendering the CB more reductive and the VB more oxidative in nature. In the second stage, the photogenerated charge carriers undergo separation and migration toward the active sites on the photocatalyst surface. Efficient charge transport is crucial at this stage, as rapid electron hole recombination significantly diminishes photocatalytic efficiency. Finally, surface redox reactions occur, wherein the photogenerated holes oxidize water molecules to produce oxygen, while the electrons reduce protons to generate hydrogen gas, as described by Eqs. (1) and (2):

$$H_2O + 2h^+ \rightarrow 2H^+ + ½O_2 \quad (1)$$

$$2H^+ + 2e^- \rightarrow H_2 \quad (2)$$

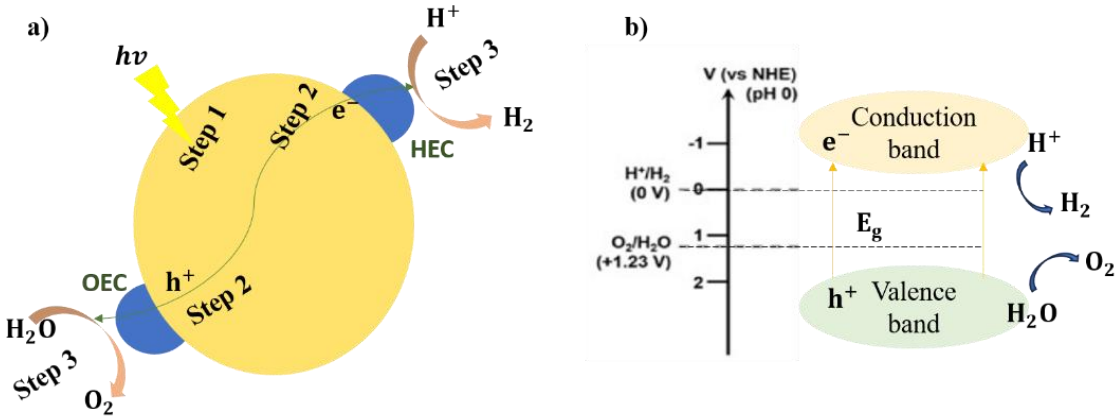


Figure 6 (a) Photocatalytic splitting of H_2O involves (i) light absorption, (ii) charge migration, (iii) redox reaction. (b) Energy diagram of one step excitation upon light absorption.

These processes are further clarified by the energy band diagram shown in **Figure 6** which depicts the energetic alignment required for successful water splitting upon light absorption. One of the major limitations in photocatalytic hydrogen production is the rapid recombination of photogenerated electron hole pairs, which severely reduces reaction efficiency. To mitigate this issue, hole scavengers are often introduced to selectively consume photogenerated holes, thereby prolonging electron lifetime and enhancing hydrogen evolution [88]. In this study, methylene blue is employed as a hole scavenger, serving a dual function: suppressing charge recombination to improve hydrogen production efficiency and simultaneously enabling the degradation of organic pollutants. Similar strategies have been widely reported, demonstrating that hole scavengers play a crucial role in improving overall photocatalytic performance [89]. Furthermore, zeolite-based supports such as ZSM-5 have been recognized as effective platforms for photocatalytic systems due to their high surface area, adsorption capacity, and suitability for wastewater treatment and pollutant removal [90]. Beyond serving as a support material, the porous framework and intrinsic Brønsted acidity of ZSM-5 may facilitate reactant transport and create a favorable microenvironment for photocatalytic reactions. Although these characteristics suggest that ZSM-5 could also benefit photocatalytic hydrogen evolution, direct investigations involving BiOBr/ZSM-5 composites remain scarce. A comparison of photocatalytic hydrogen production performances reported for various catalyst systems is summarized in

Table 3, while previously reported BiOBr- and ZSM-5-based materials for photocatalytic hydrogen production are specifically presented in **Table 4**, highlighting the important role of heterostructure engineering and porous support in improving photocatalytic activity.

Table 3 Reported photocatalytic performance over various catalyst for hydrogen production.

No	Photocatalytic Material	Strategies	Application	Result	Ref
1	TiO_2 (modified)	CuO_x modification and thermal treatment (calcination)	Photocatalytic water splitting (UV-Vis irradiation)	Hydrogen evalution rate of 2.5 mmol g^{-1} h^{-1}	[91]
2	$SrTiO_3$/g-C_3N_4/ZnO	Dual Z-scheme heterojunction construction	Overall photocatalytic water splitting	H_2 evolution rate of 603.94 μmol g^{-1} h	[92]
3	g-C_3N_4	Defect engineering	Visible light driven photocatalytic H_2 evolution	Hydrogen production rate pf 1.2 mmol g^{-1} h^{-1}	[93]
4	TiO_2/g-C_3N_4	Heterojunction	Photocatalytic hydrogen evolution	H_2 evalution enchanced by 3 - 4 times compared with single components	[94]
5	$Cd_{0.4}Zn_{0.6}S/TiO_2$	Heterojunction	Photocatalytc water splitting	Hydrogen generation rate of 1.8 mmol g^{-1} h^{-1}	[95]
6	$Znln_2S_4$ based photocatalyst	heterojunction construction	Visible light photocatalytic water splitting	High hydrogen evolution rate exceeding 4.5 mmol g^{-1} h^{-1}	[96]
7	C-doped g-C_3N_4	Carbon doping using carbon quantum dots (CQDs)	Photocatalytic water splitting	Hydrogen production efficiency improved by 0.6 mmol g^{-1} h^{-1}	[97]
8	Pt-loaded $CaTaO_2N$	Pt cocatalyst loading	Cocatalyst assited photocatalytic H_2 evolution	Hydrogen evolution rate 6.4 μmol H_2 h^{-1}	[98]
9	g-C_3N_4/TiO_2 nanotube	Z-scheme heterojunction	Photocatalytic hydrogen generation	Hydrogen production enhanced by 5 times compared with TiO_2	[99]
10	Au-Pd/g-C_3N_4 composite	Defect engineering	Cocatalyst engineered photocatalysis	High hydrogen evolution rate 5.089 mmol g^{-1} h^{-1}	[100]
11	Nd/La substituted Co-Ni oxide	Nd/La co-doping	Photocatalytic water splitting	Hydrogen production rate of 2.8 mmol g^{-1} h^{-1}	[101]

Table 3 summarizes the photocatalytic performance of various semiconductor-based materials for hydrogen production and demonstrates the strong potential of photocatalysis as a promising approach for sustainable hydrogen generation. As shown in the table, a wide range of photocatalytic materials, including TiO_2^-, g-$C_3N_4^-$, $ZnIn_2S_4^-$, $SrTiO_3^-$, $Cd_{0.4}Zn_{0.6}S$-, and metal oxide-based systems, have been successfully developed to promote hydrogen evolution under light irradiation. The reported hydrogen production rates reach the mmol g^{-1} h^{-1}range, with hydrogen evolution rates of 2.5 mmol g^{-1} h^{-1} for modified TiO_2, 1.2 mmol

g^{-1} h^{-1} for defect-engineered g-C_3N_4, 1.8 mmol g^{-1} h^{-1} for $Cd_{0.4}Zn_{0.6}S/TiO_2$, 4.5 mmolg^{-1} h^{-1}or $ZnIn_2S_4$-based photocatalysts, 5.089 mmol g^{-1} h^{-1} for Au-Pd/g-C_3N_4, and 2.8 mmolg^{-1} h^{-1} for Nd/La-substituted Co–Ni oxide. These results clearly indicate that photocatalytic systems can achieve substantial hydrogen production under light irradiation, highlighting their potential as an environmentally friendly and sustainable alternative for hydrogen generation.

The comparison in **Table 3** further demonstrates that the photocatalytic performance can be significantly improved through rational catalyst engineering. Several strategies, including heterojunction construction, Z-scheme formation, defect engineering, elemental doping, and cocatalyst loading, have been employed to overcome the intrinsic limitations of individual photocatalysts. For instance, the TiO_2/g-C_3N_4 heterojunction and TiO_2/g-C_3N_4 nanotube Z-scheme showed hydrogen evolution enhancements of approximately 3 - 4 and 5 times, respectively, compared with their corresponding single components. Similarly, the dual Z-scheme $SrTiO_3$/g-C_3N_4/ZnO system achieved a hydrogen evolution rate of 603.94 μmol g^{-1} h^{-1}, demonstrating the effectiveness of constructing multi-component photocatalytic systems for improving charge separation. The Au-Pd/g-C_3N_4 composite also exhibited a high hydrogen evolution rate of 5.089 mmol g^{-1} h^{-1}, indicating that the incorporation of suitable cocatalyst components can facilitate surface reactions and enhance the utilization of photogenerated charge carriers.

Overall, the results presented in **Table 3** demonstrate that photocatalysis is a highly promising technology for hydrogen production, while the development of advanced photocatalytic materials is essential for further improving hydrogen evolution efficiency. The improved performance observed after heterojunction formation, doping, defect engineering, and cocatalyst incorporation indicates that enhanced light harvesting, efficient separation and migration of photogenerated charge carriers, and accelerated surface reaction kinetics are key factors governing photocatalytic hydrogen production. Although the reported systems employ different materials and modification strategies, the consistent improvement in hydrogen evolution across various photocatalytic platforms highlights the versatility and potential of photocatalysis for sustainable hydrogen generation. Therefore, continued development of engineered photocatalysts with improved charge separation, enhanced light utilization, and stable catalytic activity is expected to contribute significantly to the advancement of photocatalytic hydrogen production technologies.

Table 4 Representative BiOBr-based and ZSM-5 materials for photocatalyst hydrogen production.

No	Photocatalytic Material	Strategies	Method	Result	Ref
1	α-Fe_2O_3/BiOBr/MoS_2	Heterojunction contruction	Hydrothermal	57 mmol g^{-1} h^{-1} H_2 evolution under visible light	[102]
2	Mo/S dopped BiOBr	Defect & dopant engineering	Hydrothermal	710.5 μmol h^{-1} hydrogen evolution	[103]
3	BiOBr/$Bi_{24}O_{31}Br_{10}$/ Ti_3C_2	Heterojunction contruction	Solvothermal	12.56 μmol g^{-1} h^{-1} hydrogen evolution	[104]
4	TiO_2/BiOBr p-n heterjunction	Heterojunction contruction	Solvothermal	472.7 μmol g^{-1} h^{-1} hydrogen evolution	[105]
5	BiOBr/TiO_2	Heterojunction contruction	Sono-precipitation	3.7 mmol g^{-1} h^{-1} hydrogen evolution	[106]
6	$BiVO_4$/BiOBr	Heterojunction contruction	Successive ionic layer adsorption and reaction	Enhanced photocurrent 3.2× water splitting effeciency	[107]

No	Photocatalytic Material	Strategies	Method	Result	Ref
7	Oxygen vacancy rich BiOBr	Defect induced photocatalysis	One-step alcoholysis	H_2 evolution increase 4.1×	[108]
8	Bi/MoS_2 Z-scheme	Z-scheme	Solvothermal	21.4 mmol g^{-1} h^{-1} hydrogen evolution under visible light	[109]
9	g-C_3N_4/H-ZSM-5	Heterojunction contraction	Thermal polymerization	13× increase in H_2 production	[110]

As summarized in **Table 4**, the photocatalytic performance of BiOBr-based materials can be enhanced through several approaches, including heterojunction construction, defect and dopant engineering, Z-scheme formation. Among the reported synthesis routes, hydrothermal and solvothermal methods have demonstrated strong applicability for constructing BiOBr-based heterostructures, achieving H_2 evolution rates of up to 57 and 21.4 mmol g^{-1} h^{-1}, respectively. Other methods, including sono-precipitation, SILAR, one-step alcoholysis, and thermal polymerization, have also been successfully employed to modify BiOBr-based systems and enhance H_2 production or water-splitting performance. These findings demonstrate that the selection of an appropriate synthesis route and modification strategy is critical for tailoring the photocatalytic properties of BiOBr-based materials and provide a basis for further development of BiOBr/ZSM-5-containing photocatalytic systems.

As summarized in **Tables 3** and **4**, photocatalytic hydrogen production has been successfully achieved using a wide range of semiconductor materials and various modification strategies. **Table 3** demonstrates that heterojunction construction, cocatalyst loading, and defect engineering have enhanced hydrogen evolution performance in numerous photocatalytic systems. Likewise, **Table 4** indicates that BiOBr-based photocatalysts exhibit considerable potential for hydrogen evolution, particularly when modified through heterojunction construction, defect engineering. These studies demonstrate that the intrinsic photocatalytic properties of BiOBr can be effectively enhanced to improve charge separation and surface reaction kinetics, resulting in improved hydrogen production performance. However, studies investigating BiOBr/ZSM-5 composites for photocatalytic hydrogen production remain very limited. Although the application of ZSM-5 has been extensively explored as a porous support in photocatalytic pollutant degradation, its integration with BiOBr for hydrogen evolution has received little attention. Considering the demonstrated hydrogen evolution capability of BiOBr-based photocatalysts and the well-established role of ZSM-5 as a porous support possessing high surface area, excellent adsorption capacity, interconnected microporous channels, and Brønsted acid sites, integrating these 2 materials represents a scientifically promising strategy that deserves further investigation. Therefore, BiOBr/ZSM-5 composites may provide new opportunities for hydrogen production and environmental remediation, although direct experimental validation is still required.

Based on the complementary physicochemical properties of BiOBr and ZSM-5, a hypothetical mechanism for photocatalytic hydrogen evolution over the BiOBr/ZSM-5 composite can be proposed. BiOBr is considered a promising visible-light-responsive photocatalyst because of its suitable band gap, layered crystal structure, and intrinsic internal electric field generated by the alternating $[Bi_2O_2]^{2+}$ and Br^- layers [111]. These characteristics facilitate the generation and separation of photogenerated charge carriers, providing the fundamental basis for photocatalytic hydrogen evolution. Upon visible-light irradiation, BiOBr absorbs photons with energy equal to or greater than its band gap, promoting electrons from the valence band (VB) to the conduction band (CB) and generating electron–hole pairs [112].

In the BiOBr/ZSM-5 composite, the intimate interfacial contact between BiOBr and the ZSM-5 framework is expected to facilitate the spatial separation and migration of photogenerated charge carriers,

thereby suppressing electron–hole recombination. The porous MFI framework of ZSM-5 provides a high external surface area that promotes uniform dispersion of BiOBr particles while facilitating the diffusion of water molecules and reaction intermediates toward the photocatalytic active sites. Unlike inert supports, ZSM-5 also possesses Brønsted acid sites originating from framework aluminum atoms. These acidic sites may adsorb and stabilize proton-containing species, creating a localized proton-rich microenvironment adjacent to the BiOBr surface [113]. Such proton enrichment is expected to shorten proton diffusion distances and increase the probability of proton reduction by photogenerated electrons, thereby promoting hydrogen evolution [114].

Following the improved charge separation, the accumulated photogenerated electrons in the conduction band of BiOBr can participate in the reduction of H^+ to molecular hydrogen ($2H^+ + 2e^- \rightarrow H_2$), provided that the conduction band potential is thermodynamically favorable for proton reduction [105]. Meanwhile, the photogenerated holes remaining in the valence band participate in water oxidation or are consumed by sacrificial agents, thereby maintaining charge neutrality and prolonging electron lifetime [33]. During in wastewater treatment, adsorbed organic pollutants on the ZSM-5 surface may also function as hole scavengers, further suppressing electron–hole recombination and increasing the availability of electrons for hydrogen evolution [115]. Consequently, BiOBr primarily functions as the visible-light-responsive photocatalyst responsible for photon absorption and charge generation, whereas ZSM-5 acts as a multifunctional support that enhances charge separation, facilitates reactant transport, enriches local proton concentration, and suppresses charge recombination through its porous and acidic framework.

ZSM-5 in photocatalysis

ZSM-5 is an MFI type zeolite that has been widely employed in modern photocatalytic systems due to its unique structural and physicochemical characteristics, including a 3-dimensional microporous network composed of straight and sinusoidal ten membered ring channels, high surface area, tunable acidity controlled by the Si/Al ratio, and excellent thermal and chemical stability (**Table 5**) [116-118]. Although ZSM-5 is not a semiconductor and does not directly participate in light absorption, its contribution to photocatalysis is fundamental and systemic [119,120]. It acts as a functional matrix that governs adsorption behavior, dispersion of active phases, charge transfer, reactant diffusion, and overall catalyst stability [121,122]. In composite photocatalytic systems, ZSM-5 serves as an effective support capable of homogeneously dispersing semiconductor particles or metal species on its external surface and within its pore system, thereby suppressing agglomeration, increasing effective surface area, and maintaining the accessibility of active sites to both light and reactants [123,124]. Moreover, the strong adsorption capacity of ZSM-5 enables the pre-concentration of organic pollutants near the photocatalytic phase, creating a synergistic adsorption photodegradation effect that significantly enhances reaction kinetics and reactive species utilization efficiency [125].

Table 5 Typical physicochemical properties of ZSM-5 zeolite [128].

Property	Typical Value	Description
Chemical formula	$M_{x/n}[(Al_2)_x(SiO_2)_y] \cdot {}_mH_2O$	M represents the exchangeable cation, n = number of Al atoms per unit cell (Si/Al ratio dependent), and m is the number of water molecules.
Framework type	MFI	As per the IZA zeolite framework code
Crystal structure	Orthorombic	Chennerks formed by intersecting 10-membered rings
Si/Al ratio	10-∞	Higher ratios show more hydrophobicity, lower acidity

Property	Typical Value	Description
Pore size	5.1 - 5.6×5.3 - 5.6 $Å^2$	Elliptical 10-membered rings pores
Surface area	300 - 450 m^2/g	Depends in synthesis and calcination
Micropore volume	0.18 - 0.24 cm^3/g	Form N_2 adsorption
Crystal size	100 nm	Tuned by synthesisi conditions
Density	1.79 g/cm^3	Framework density
Acidity	Bronsted and lewis sties	Si-OH-Al groups; Lewis form extra-framework metals
Thermal stability	Up to 800 - 1,000 ℃	Stable in oxidative atmosphere
Hydrophobicity	Increases with Si/Al ratio	Relevant for adsorption and catalysis
Channel system	2D intersecting straight and sinusoidal chennerls	10-ring channels

Beyond its physical role, ZSM-5 also contributes chemically and mechanistically to photocatalytic processes [127]. The presence of Brønsted and Lewis acid sites within the zeolite framework facilitates molecular activation, formation of reactive intermediates, and regulation of reaction pathways, which can synergize with photocatalytic electron hole processes [128]. In several hybrid systems, the acidity of ZSM-5 has been reported to indirectly promote charge separation and suppress electron hole recombination through interfacial interactions between the zeolite and semiconductor phases [129,130]. Furthermore, modification of ZSM-5 via ion exchange, transition metal doping, or the creation of isolated metal sites offers opportunities to generate electron-trapping centers that prolong charge-carrier lifetimes and enhance the formation of reactive oxidative species such as ·OH and $\cdot O_2^+$. These features highlight the active role of ZSM-5 in governing photocatalytic efficiency at the mechanistic level [131,132].

Radoor *et al.* [133] have reported the synthesis of mesoporous ZSM-5 zeolite via a hydrothermal method for the removal of methyl orange (MO) from aqueous media. The successful introduction of mesoporosity through cellulose modification was confirmed by SEM and N_2 adsorption desorption analyses. The synthesized mesoporous ZSM-5 exhibited good crystallinity and thermal stability, which are favorable characteristics for adsorption-based dye removal. Compared to conventional ZSM-5, the mesoporous structure demonstrated enhanced adsorption performance toward MO. The adsorption behavior was strongly affected by operational parameters such as initial dye concentration, adsorbent dosage, temperature, pH, and contact time. An increase in adsorption capacity was observed with increasing dye concentration, adsorbent dosage, and temperature, while higher pH values led to decreased adsorption efficiency. Equilibrium data were best described by the Freundlich isotherm model, with a maximum adsorption capacity of 5.5 mg g^{-1}, indicating heterogeneous surface adsorption. Kinetic studies revealed that the adsorption process followed a pseudo second order model. Moreover, the mesoporous ZSM-5 showed good regeneration ability, highlighting its potential as an efficient adsorbent for the removal of toxic azo dyes from wastewater [133].

From a materials engineering perspective, the structural flexibility of ZSM-5 enables the development of advanced photocatalytic architectures, including zeolite semiconductor composites, hierarchical micro-mesoporous materials, and immobilized or granular systems. In such configurations, ZSM-5 acts as a regulator of diffusion and reaction environment, where pore size, channel connectivity, and particle morphology influence mass transport of reactants and products, particularly in liquid-phase photocatalysis. These advantages are highly relevant for practical applications, as ZSM-5 enhances structural stability under repeated irradiation, suppresses leaching of active phases, and facilitates catalyst separation and regeneration. Consequently, ZSM-5 addresses key limitations associated with conventional nanoparticulate

photocatalysts, especially in terms of durability and recyclability. Representative examples of ZSM-5-based composite photocatalysts, their photocatalytic applications, and their performance under visible-light irradiation are summarized in **Table 6**.

Table 6 Reported ZSM-5 based composite photocatalysts, their photocatalytic applications, and performance under visible light irradiation.

No.	Material	Photocatalytic Application	Result	Ref
1	ZSM-5/ZnO/Ag	MO degradation (UV–Vis)	95% - 98% MO removal within 60 min; higher rate than ZnO	[134]
2	ZSM-5/Fly ash/TiO_2/Cu	Crystal violet degradation	90% removal under visible/solar light in 120 min	[135]
3	TiO_2/Ni/ZSM-5	Dye degradation	85% - 90% dye removal; significant PL quenching vs TiO_2	[114]
4	TiO_2–NiO/ZSM-5	RhB degradation	93% degradation in 60 min; improved cycling stability	[136]
5	TiO_2/ZSM-5	Azo dye degradation	80% - 90% decolorization; adsorption + photocatalysis synergy	[137]
6	ZnO/ZSM-5	CO_2 photocatalytic reduction	CO_2 → CH_3OH yield increased = 1.5 - 2× vs ZnO	[138]
7	Hierarchical Zn-ZSM-5	MB degradation	92% - 95% MB removal within 50 - 60 min	[139]
8	CdS/PANI/ZSM-5 hollow spheres	SBX degradation (visible light)	88% - 90% degradation; enhanced stability over 5 cycles	[140]
9	TiO_2/g-C_3N_4@ZSM-5	Organic dye degradation	96% removal; Z-scheme enhances charge separation	[141]
10	Ag/ZSM-5/g-C_3N_4/TiO_2	Formaldehyde degradation	70% - 80% HCHO removal under visible light	[142]
11	Polythiophene/ZSM-5	CO_2 photoreduction	CO_2 conversion increased 2× vs polymer alone	[143]
12	BiOBr/ZSM-5	RhB / MB degradation	90% - 98% degradation under visible light	[24]
13	Ag/ZnO/ZSM-5	4-nitrophenol	97% - 99% 4-nitrophenol removal	[144]
14	Multicomponent heterojunction/ZSM-5	Organic pollutant degradation	Reaction rate enhanced 2 - 3× vs single component	[145]
15	Fe-ZSM-5@TiO_2-Ag	Dye degradation	94% - 96% removal; high recyclability (> 5 cycles)	[146]

Overall, the role of ZSM-5 in photocatalysis should be viewed as an integral part of system level photocatalyst design rather than merely as a passive support as summarized in **Table 6**. Its integration enables control over structural and chemical interfacial interactions, enhances reaction efficiency through adsorption photocatalysis synergy, and supports the development of stable, reusable, and application-oriented photocatalytic systems. Therefore, ZSM-5 occupies a pivotal position in the evolution of next-generation hybrid photocatalysts, particularly in bridging the gap between laboratory scale performance and large-scale practical implementation for

environmental remediation and sustainable chemical conversion.

Potential of BiOBr/ZSM-5 photocatalyst

The development of Bi-based photocatalysts supported on ZSM-5 has been strongly influenced by early studies emphasizing the adsorptive function of zeolite matrices. In particular, the Zeolite/Bi_2O_3 nanocomposite synthesized via a sol gel route demonstrated complete removal of Rhodamine B through multilayer adsorption and chemisorption mechanisms, as confirmed by Freundlich isotherms and pseudo-second-order kinetics [147]. This study clearly showed that the high surface area and pore structure of zeolite enable effective pre-concentration of dye molecules at the solid liquid interface [147]. Similar conclusions were drawn from adsorption-focused studies on zeolite and biomaterial-based systems, which emphasized that surface chemistry and pore accessibility dominate adsorption performance [148]. Although these systems were not photoactive, they provided a critical foundation for integrating adsorption and photocatalysis within a single hybrid material [147,148]. Study by Utomo *et al.* [24] show that BiOBr exhibited good photocatalytic activity for methylene blue degradation, and its performance was significantly enhanced after coupling with ZSM-5. BiOBr synthesized via a coprecipitation method at room temperature achieved a methylene blue degradation efficiency of 50.96% after 120 min of UV irradiation, which was higher than that of irregular pure BiOBr, reaching only 31.82%. After compositing with ZSM-5, the photocatalytic efficiency further increased to 87.29%. This enhanced performance was attributed to the role of ZSM-5 in improving pollutant adsorption and facilitating charge transfer as well as electron–hole separation, thereby reducing charge recombination in BiOBr. These results demonstrate that the formation of a BiOBr/ZSM-5 composite is an effective strategy to improve the photocatalytic performance of BiOBr for organic dye degradation [24].

A more fundamental understanding of Bi zeolite interactions was provided by the high-pressure high-temperature insertion of Bi^{3+} into silicalite-1 (MFI), where bismuth atoms were successfully incorporated into the zeolite framework without destroying crystallinity [149]. Spectroscopic evidence from extended X-ray absorption fine structure (EXAFS) and X-ray abroption near edge structure (XANES) confirmed that Bi occupied tetrahedrally coordinated sites within the framework, forming stable Bi–O–Si linkages [149]. This finding demonstrated that the interaction between bismuth species and zeolite can extend beyond surface deposition to structural integration [149]. Although this approach is impractical for large scale environmental applications, it offers important theoretical insight into interfacial electronic modification in Bi zeolite systems [149]. These insights are directly relevant to BiOBr/ZSM-5 composites, where strong interfacial bonding is expected to influence charge transfer behavior [150].

The transition from adsorption dominated systems to photocatalytic active materials was realized through Bi based oxide/zeolite composites synthesized by hydrothermal or impregnation methods. These studies reported enhanced dispersion of Bi based semiconductors and suppressed electron hole recombination when zeolites were used as supports [113]. Photoluminescence and electrochemical impedance spectroscopy further confirmed that zeolite-assisted interfaces promote more efficient charge separation and transfer [113,151]. A conceptual review comparing adsorption and photocatalysis in zeolite Bi composites concluded that adsorption dominates the initial pollutant uptake, while photocatalysis governs subsequent degradation and mineralization processes [152]. Consequently, hybrid zeolite Bi materials were identified as superior systems compared to single-function adsorbents or photocatalysts.

A major breakthrough in Bi based oxohalide/zeolite systems was achieved with the *in-situ* precipitation synthesis of $Bi_4O_5Br_2$ doped ZSM-5. Study by Zhang *et al.* [152] composite exhibited nearly complete degradation of Rhodamine B (99.86%) within 25 minutes under visible light irradiation, with a reaction rate constant 2.32 times higher than that of pristine $Bi_4O_5Br_2$. The remarkable performance was attributed to a 4-fold increase in surface area and the formation of efficient interfacial charge-transfer pathways between $Bi_4O_5Br_2$ and ZSM-5. Photocurrent, PL, and electron impedance spectroscopy (EIS) analyses clearly demonstrated that ZSM-5 actively facilitated electron migration and suppressed charge recombination. This study provided strong experimental

evidence that ZSM-5 functions as an electronic mediator rather than a passive support in Bi-based photocatalysts [152]. UV–Vis diffuse reflectance spectroscopy (DRS) results show that $Bi_4O_5Br_2$ exhibits light absorption from the UV to the visible region with a maximum wavelength of approximately 476 nm. After being composited with ZSM-5 (1ZSM/ $Bi_4O_5Br_2$), a red shift toward a longer wavelength is observed along with an increase in absorption intensity. This phenomenon indicates strong electronic interaction and coupling between ZSM-5 and $Bi_4O_5Br_2$, which enhances the material's ability to utilize visible light for generating electron–hole pairs. The band gap results show that the energy band gap of $Bi_4O_5Br_2$ is approximately 2.31 eV, while that of the 1ZSM/ $Bi_4O_5Br_2$ composite decreases to around 2.21 eV. This reduction indicates that the composite can be more easily excited under visible light irradiation PL intensity of 1ZSM/ $Bi_4O_5Br_2$ is significantly lower than that of pure $Bi_4O_5Br_2$, indicating that the electron–hole recombination rate is effectively suppressed. Overall, the enhanced light absorption, reduced band gap, and decreased charge carrier recombination demonstrate that the incorporation of ZSM-5 significantly improves the photocatalytic performance of the material.

In photocurrent analysis shows that 1ZSM/ $Bi_4O_5Br_2$ exhibits a much higher photocurrent density compared to pure $Bi_4O_5Br_2$, indicating a more efficient separation of photogenerated electron–hole pairs and enhanced charge transfer under light irradiation. The current response increases when the light is turned on and quickly returns to its initial state when the light is off, confirming good photoresponsivity of the materials. The higher photocurrent of the composite is attributed to the strong interfacial interaction between ZSM-5 and $Bi_4O_5Br_2$, which facilitates faster electron migration and reduces charge recombination. EIS further supports this result, where the Tauch plot of 1ZSM/ $Bi_4O_5Br_2$ shows a smaller semicircle radius compared to $Bi_4O_5Br_2$. This indicates lower charge transfer resistance and more efficient interfacial charge transport in the composite. Overall, both PC and EIS results confirm that the incorporation of ZSM-5 significantly improves the separation and migration of photogenerated carriers, leading to enhanced photocatalytic performance [152].

Similar synergistic effects have been observed in several BiOBr/ZSM-5 composites developed for visible light driven dye degradation. These systems exhibited reduced band-gap energies and enhanced photocatalytic activity toward MB, MO, and RhB compared with pristine BiOBr [151]. The improved performance was attributed to dual-function behavior, where ZSM-5 enhances dye adsorption and BiOBr serves as the primary photoactive phase [153]. Furthermore, the formation of internal heterojunctions was shown to effectively inhibit electron hole recombination. However, some studies lacked comprehensive radical scavenging experiments, limiting mechanistic verification of active species pathways. A recent study by Nyakairu *et al.* [147] synthesized a Zeolite/Bi_2O_3 nanocomposite via a sol–gel method for Rhodamine B removal from wastewater. The composite exhibited excellent photocatalytic performance, achieving complete Rhodamine B removal under optimized conditions and maintaining high removal efficiency (98.12%) in real wastewater with good reusability over multiple cycles. These findings demonstrate that integrating bismuth oxide with a zeolite support effectively combines the adsorption capability of zeolite with the photocatalytic activity of bismuth-based semiconductors, resulting in enhanced pollutant removal. Therefore, the successful development of the Bi_2O_3/ZSM-5 system provides a valuable foundation for extending this strategy to BiOBr/ZSM-5 composites, where the superior visible-light response of BiOBr is expected to further improve photocatalytic performance for environmental applications.

Based on the reported studies, different synthesis methods offer distinct advantages for developing Bi-based/ZSM-5 photocatalysts. The sol–gel method produces homogeneous composites with excellent adsorption capability, making it effective for pollutant removal through adsorption–photocatalysis synergy. Coprecipitation has emerged as a promising synthesis route for BiOBr/ZSM-5 because it can be performed under mild conditions while producing well-dispersed BiOBr particles on the ZSM-5 surface, resulting in enhanced photocatalytic degradation. Meanwhile, in-situ precipitation has demonstrated excellent photocatalytic performance in $Bi_4O_5Br_2$/ZSM-5 by promoting intimate semiconductor–zeolite contact and rapid pollutant degradation. Although this strategy has not yet been applied to BiOBr/ZSM-5, its successful implementation in other Bi-based/zeolite systems

suggests considerable potential for future adaptation. Therefore, coprecipitation currently represents the most practical synthesis route for BiOBr/ZSM-5, whereas adapting in-situ precipitation may provide a promising strategy for further improving photocatalytic performance.

To further demonstrate the applicability of the coprecipitation strategy for BiOBr/ZSM-5, our research group developed a facile room-temperature coprecipitation method using polyvinyl pyrrolidone (PVP) as a capping agent to synthesize flower-shaped BiOBr nanosheets (BP) [24]. The SEM images reveal the formation of hierarchical flower-like BiOBr structures composed of ultrathin nanosheets, and in images SEM confirms the successful anchoring of BiOBr onto the porous ZSM-5 framework to form the BiOBr/PVP/ZSM-5 composite (BPZ). Furthermore, the UV–Vis DRS spectra demonstrate that the BPZ composite exhibits enhanced light absorption compared to pristine BiOBr, indicating improved light harvesting capability. The corresponding band gap analysis also reveals a reduction in band gap energy after the incorporation of ZSM-5 and PVP, which facilitates better visible-light utilization. In addition, the photocatalytic degradation performance and kinetic plots show that the BPZ composite achieved 87.29% methylene blue degradation within 120 minutes under UV-LED irradiation (365 nm, 12×2 W), significantly outperforming pristine BiOBr (31.82%) and PVP-modified BiOBr without ZSM-5 (50.96%). The presence of PVP effectively regulated crystal growth, resulting in ultrathin nanosheets with reduced charge recombination, while the porous ZSM-5 support enhanced pollutant adsorption and facilitated interfacial electron transfer. This study demonstrated a strong synergistic effect between morphology control and surface anchoring, achieved through a simple, low energy, and scalable synthesis protocol suitable for environmental applications [24].

Overall, the reported studies demonstrate that the synthesis strategy is a key factor governing the performance of BiOBr/ZSM-5 photocatalysts. Appropriate synthesis methods promote better semiconductor–zeolite interaction, leading to enhanced adsorption, improved photocatalytic activity, and more efficient utilization of the active sites. Therefore, further optimization of synthesis strategies and interfacial engineering is expected to play a crucial role in developing high-performance BiOBr/ZSM-5 photocatalysts for sustainable environmental remediation.

Perspective and outlooks

Although considerable progress has been achieved in the development of BiOBr/ZSM-5 photocatalysts for environmental remediation, several scientific and technological challenges remain before their practical implementation can be realized. Future research should shift from empirical material optimization toward mechanism-driven design by establishing clear relationships between synthesis strategy, interfacial structure, charge-transfer behavior, and photocatalytic performance. In particular, systematic comparisons of synthesis routes, including coprecipitation, hydrothermal, and emerging in-situ growth approaches, are needed to identify the most effective strategy for constructing robust semiconductor–zeolite interfaces.

The multifunctional role of ZSM-5 also deserves further investigation. Beyond serving as a high-surface-area support, future studies should clarify how framework acidity, Si/Al ratio, pore architecture, and surface chemistry influence pollutant adsorption, interfacial charge transfer, and proton transport during photocatalytic reactions. Rational engineering of these properties is expected to strengthen the synergistic interaction between BiOBr and ZSM-5, leading to improved photocatalytic efficiency and catalyst stability.

Despite the excellent performance of BiOBr/ZSM-5 for pollutant degradation, its application in photocatalytic hydrogen production remains largely unexplored. Future studies should therefore focus on developing BiOBr/ZSM-5 systems for hydrogen evolution through strategies such as cocatalyst loading, heterojunction engineering, and defect engineering. Particular attention should be given to experimentally verifying the proposed role of ZSM-5 in facilitating proton transport and interfacial charge separation, as well as evaluating hydrogen production under sacrificial-agent-free conditions and simulated solar irradiation.

From an application perspective, future research should also prioritize the development of structured and granulated BiOBr/ZSM-5 photocatalysts with improved

mechanical stability, recyclability, and ease of recovery. Furthermore, advanced operando characterization techniques, including in-situ XPS, transient spectroscopy, and operando FTIR, combined with density functional theory calculations, are required to reveal the dynamic interfacial processes governing photocatalytic activity. Finally, techno-economic assessment, long-term stability evaluation, and performance validation in real wastewater systems should be incorporated into future studies to accelerate the transition of BiOBr/ZSM-5 photocatalysts from laboratory-scale research toward practical environmental remediation and sustainable hydrogen production.

Conclusions

BiOBr/ZSM-5 composites have emerged as promising visible-light-responsive photocatalysts by integrating the photocatalytic activity of BiOBr with the adsorption capability and porous framework of ZSM-5. The reviewed literature demonstrates that photocatalytic performance is strongly governed by synthesis strategy, morphology, and interfacial interaction between BiOBr and ZSM-5. Among the reported approaches, coprecipitation has proven to be a simple and effective route for fabricating BiOBr/ZSM-5 composites with enhanced photocatalytic performance, while hierarchical flower-like BiOBr nanosheets anchored on ZSM-5 have exhibited superior activity due to improved light harvesting, pollutant adsorption, and charge separation. Consequently, BiOBr/ZSM-5 composites have achieved methylene blue degradation efficiencies of up to 87.29%, highlighting the effectiveness of integrating adsorption and photocatalysis within a single material. Despite these advances, the application of BiOBr/ZSM-5 composites for photocatalytic hydrogen production remains largely unexplored. Future research should therefore focus on rational interface engineering, optimization of synthesis strategies, and experimental verification of charge-transfer mechanisms to fully exploit the potential of BiOBr/ZSM-5 photocatalysts for sustainable environmental remediation and hydrogen production.

Acknowledgements

This research is funded by the Indonesian Endowment Fund for Education (LPDP) on behalf of the Indonesian Ministry of Higher Education, Science and Technology and managed under the EQUITY program (Contract No. 4299/B3/DT.03.08/2025 & No 3029/PKS/ITS/2025).

Declaration of generative AI in scientific writing

The authors acknowledge the use of generative AI tool (e.g ChatGPT by OpenAI) for language editing and grammar correction. No content generation or data interpretation was performed by AI. The authors take full responsibility for the content and conclusions of this work.

CRediT author statement

Revvara Khusuma: conceptualization, literature search and data analysis, visualization, writing – original draft. **Wahyu Prasetyo Utomo:** conceptualization, literature search and data analysis, supervision, resources, writing – review & editing. **Nor Farida:** visualization, validation. **Ade Irma Rozafia:** Formal analysis, validation. **Zjahra Vianita Nugraheni:** Formal analysis, validation. **Hao Wu:** resources, writing – review & editing. **Zhi Zhu:** validation, writing – review & editing. **Djoko Hartanto:** Supervision, validation, writing – review & editing**.**

References

[1] Y Li, H Jiang, X Wang, X Hong and B Liang. Recent advances in bismuth oxyhalide photocatalysts for degradation of organic pollutants in wastewater. *RSC Advances* 2021; **11(43)**, 26855-26875.

[2] A Geng, L Xu, L Gan, C Mei, L Wang, X Fang, M Li, M Pan, S Han and J Cui. Using wood flour waste to produce biochar as the support to enhance the visible-light photocatalytic performance of BiOBr for organic and inorganic contaminants removal. *Chemosphere* 2020; **250**, 126291.

[3] LL Zulfa, ARP Hidayat, BTI Ali, WP Utomo, EN Kusumawati, D Hartanto and R Ediati. Enhanced photocatalytic degradation of methylene blue using bimetallic C,N-doped NiO/ZnO derived from metal-organic frameworks. *Materials Today Chemistry* 2025; **43**, 102489.

[4] S Saquib, H Julian, SH Suhardi, T Watari, T Yamaguchi and T Setiadi. Optimizing dye

wastewater treatment: The impact of operational flux in submerged anaerobic membrane bioreactor. *South African Journal of Chemical Engineering* 2024; **49**, 210-222.

[5] WP Utomo, PAI Afifah, AI Rozafia, AA Mahardika, E Santoso, R Liu and D Hartanto. Modulation of particle size and morphology of zinc oxide in graphitic carbon nitride/zinc oxide composites for enhanced photocatalytic degradation of methylene blue. *Surfaces and Interfaces* 2024; **46**, 104017.

[6] K Kuśmierek, L Dąbek and A Świątkowski. The influence of the shape and grain size of commercial activated carbons on their sorption efficiency towards organic water pollutants. *Desalination and Water Treatment* 2025; **321**, 100996.

[7] N Karimah, RC Andiani, WP Utomo, AI Rozafia, N Farida, A Rosyidah, R Liu, Q Xu and D Hartanto. Factors contributing to reduced photocatalytic activity in Cu-loaded TiO_2/activated carbon composites for methylene blue degradation. *South African Journal of Chemical Engineering* 2025; **54**, 582-596.

[8] A Hayat, AG Al-Sehemi, KS El-Nasser, TA Taha, AA Al-Ghamdi, JAS Syed, MA Amin, T Ali, T Bashir, A Palamanit, J Khan and WI Nawawi. Graphitic carbon nitride ($g–C_3N_4$)–based semiconductor as a beneficial candidate in photocatalysis diversity. *International Journal of Hydrogen Energy* 2022; **47(8)**, 5142-5191.

[9] Y Wang, H Ma, J Liu, Z Zhang, Y Yu and S Zuo. Broad-spectrum hybrid-driven triple-interface Z-Scheme 1T/2H phase sailboat-like molybdenum disulfide (MoS_2)/protonated N-defect nanoporous graphitic carbon nitride ($g-C_3N_4$) nanosheets piezo-photocatalyst: Superior degradation and hydrogen evolution. *Journal of Colloid and Interface Science* 2024; **665**, 655-680.

[10] C Yang, Y Chen, T Chen, J Low, S Rajendran, Z Zeng, X Zhang and J Qin. Active site modulation of porous $g-C_3N_4$ nanofragment via defect assemblage for enhancing visible-light driven hydrogen evolution. *Fuel* 2023; **337**, 126894.

[11] AG Abdullahi, HY Hafeez, J Mohammed, AA Bala, CE Ndikilar and AB Suleiman. Recent advancements and future perspectives for TiO2-based materials for efficient solar fuel hydrogen production via photocatalytic water splitting. *Journal of Alloys and Compounds Communications* 2025; **8**, 100108.

[12] Y Li, H Yang, J Li, Y Li, W Ren, J Wen, Q Xiao and J Xu. One-step direct construction of S-scheme $BaTi_2O_5/g-C_3N_4$ heterojunction for enhanced photocatalytic hydrogen evolution. *Science China Materials* 2024; **67(7)**, 2142-2152.

[13] L Mohapatra, L Paramanik, D Choi and SH Yoo. Advancing photocatalytic performance for enhanced visible-light-driven H2 evolution and Cr(VI) reduction of $g-C_3N_4$ through defect engineering via electron beam irradiation. *Applied Surface Science* 2025; **685**, 161996.

[14] R Ediati, LL Zulfa, I Maulidah, DO Sulistiono, H Fansuri, A Rosyidah, F Martak, D Hartanto, MA Bakri Abdullah, WP Utomo, EN Kusumawati and M Shirai. Addition of graphene oxide to ZIF-8/HKUST-1 composite for enhanced adsorptive and photocatalytic removal of congo red in wastewater. *South African Journal of Chemical Engineering* 2023; **46(1)**, 132-142.

[15] AV Abega, C Marchal, MA Dziurla and D Robert. Investigation of a new modified easy one-step hydrothermal method to synthesize Z-scheme gC_3N_4-TiO_2 composites for enhanced photocatalytic mineralization of sodium diclofenac under simulated solar light irradiation. *Journal of Photochemistry and Photobiology A: Chemistry* 2024; **456**, 115850.

[16] LL Zulfa, R Ediati, ARP Hidayat, R Subagyo, N Faaizatunnisa, Y Kusumawati, D Hartanto, N Widiastuti, WP Utomo and M Santoso. Synergistic effect of modified pore and heterojunction of MOF-derived α-Fe_2O_3/ZnO for superior photocatalytic degradation of methylene blue. *RSC Advances* 2023; **13(6)**, 3818-3834.

[17] Y Liu, Y Zhang and L Shi. One-step synthesis of S-doped and nitrogen-defects co-modified mesoporous $g-C_3N_4$ with excellent photocatalytic hydrogen production efficiency and degradation ability. *Colloids and Surfaces A: Physicochemical and Engineering Aspects* 2022; **641**, 128577.

[18] H Xing, J Shi, Y Li and J Wu. Visible light driven generation of dual active oxygen species on Zr-MOF/$g-C_3N4$–photocatalyst for highly selective

photocatalytic oxidation of sulfides to sulfoxides. *Inorganic Chemistry Communications* 2024; **162**, 112129.

[19] A Parvees, U Priyadarshini and N Remya. Visible light induced photocatalytic degradation of methylene blue using carbon fibre cloth - Bismuth oxybromide – Water hyacinth derived silver nanocomposite. *Environmental Research* 2024; **262**, 119787.

[20] S Heng, X Lu, Y Song, Z Liu, L Hu, Y Liu, J Liu, T Cai and G Zhen. Oxygen vacancies in Z-scheme r-MIL-88A/OV-BiOBr heterojunctions enhance photo-Fenton degradation of chloroquine phosphate: Mechanisms insight, DFT calculations, degradation pathways and toxicity assessment. *Journal of Materials Science & Technology* 2024; **190**, 172-187.

[21] M Mansour, I Benyamina, B Benalioua, PDA Bentouami, PDB Boury, H Hentit and PE Lippens. Combined effect between PVP and glass wool for improvement of the photocatalytic activity under visible light of bismuth (III) oxyhalide and access to α-Bi_2O_3-BiOI-BiOBr. *Applied Surface Science* 2020; **534**, 147577.

[22] X Hou, Y Ma, W Zhang, X Zhou, Z Kang, X Hu and H Tian. Facile one-step solvothermal synthesis of flower-like BiOBr microspheres for the efficient degradation of organic dyes under visible light irradiation. *Journal of Alloys and Compounds* 2024; **997**, 174912.

[23] Y Guo, T Zhong, J Ruan and H Wen. Co-exposed crystal facets optimizing photocatalytic activity and photosensitization ability: A case of facile, fast and scalable synthesis of BiOBr round nanosheets. *Colloids and Surfaces A: Physicochemical and Engineering Aspects* 2022; **654**, 130049.

[24] WP Utomo, N Farida, B Aisyah, AA Babgei, N Karimah, AI Rozafia, I Susilo, T Widjaja, H Nur, R Sari, RJ Liu and D Hartanto. Facile synthesis of flower-like bismuth oxybromide anchored on ZSM-5 for enhanced photocatalytic dye degradation. *South African Journal of Chemical Engineering* 2025; **53**, 386-399.

[25] A Iryani, H Nur, M Santoso and D Hartanto. Adsorption Study of Rhodamine B and Methylene Blue Dyes with ZSM-5 Directly Synthesized from Bangka Kaolin without Organic Template. *Indonesian Journal of Chemistry* 2019; **20(1)**, 130.

[26] D Hartanto, R Kurniawati, AB Pambudi, WP Utomo, WL Leaw and H Nur. One-pot non-template synthesis of hierarchical ZSM-5 from kaolin source. *Solid State Sciences* 2019; **87**, 150-154.

[27] D Hartanto, G Yuhaneka, WP Utomo, AI Rozafia, Y Kusumawati, W Dahani and A Iryani. Unveiling the charge transfer behavior within ZSM-5 and carbon nitride composites for enhanced photocatalytic degradation of methylene blue. *RSC Advances* 2022; **12(9)**, 5665-5676.

[28] V Dutta, S Sharma, P Raizada, R Kumar, VK Thakur, VH Nguyen, AM Asiri, AAP Khan and P Singh. Recent progress on bismuth-based Z-scheme semiconductor photocatalysts for energy and environmental applications. *Journal of Environmental Chemical Engineering* 2020; **8(6)**, 104505.

[29] H Wang, Y Sun and F Dong. Bismuth metal and semiconductor-based photocatalysts: Structure tuning, activity enhancement, and reaction mechanism. *Interface Science and Technology* 2020; **31**, 349-377.

[30] SH Ha, SA Younis, K Vikrant, JE Szulejko and KH Kim. Evidence of the dominant role of particle size in controlling the dynamic adsorption breakthrough behavior of gaseous benzene in a microporous carbon bed system. *Chemical Engineering Journal* 2022; **427**, 130977.

[31] WP Utomo, MK Leung, Z Yin, H Wu and YH Ng. Advancement of bismuth-based materials for electrocatalytic and photo (electro) catalytic ammonia synthesis. *Advanced Functional Materials* 2022; **32(4)**, 2106713.

[32] F Shen, L Zhou, J Shi, M Xing and J Zhang. Preparation and characterization of SiO_2/BiOX (X = Cl, Br, I) films with high visible-light activity. *RSC Advances* 2015; **5(7)**, 4918-4925.

[33] Y Jia, P Liu, Q Wang, Y Wu, D Cao and QA Qiao. Construction of Bi_2S_3-BiOBr nanosheets on TiO_2 NTA as the effective photocatalysts: Pollutant removal, photoelectric conversion and hydrogen generation. *Journal of Colloid and Interface Science* 2021; **585**, 459-469.

[34] B Zhang, M Zhang, L Zhang, PA Bingham, W Li and S Kubuki. PVP surfactant-modified flower-like BiOBr with tunable bandgap structure for efficient photocatalytic decontamination of pollutants. *Applied Surface Science* 2020; **530**, 147233.

[35] C Gong, J Chu, S Qian, C Yin, X Hu, H Wang, Y Wang, X Ding, S Jiang, A Li, Y Gong, X Wang, C Li, T Zhai and J Xiong. Large-scale ultrathin 2D wide-bandgap BiOBr nanoflakes for gate-controlled deep-ultraviolet phototransistors. *Advanced Materials* 2020; **32(12)**, 1908242.

[36] F Duan, X Wang, T Tan and M Chen. Highly exposed surface area of {001} facets dominated BiOBr nanosheets with enhanced visible light photocatalytic activity. *Physical Chemistry Chemical Physics* 2016; **18(8)**, 6113-6121.

[37] S Dutta, S Adhikary, S Bhattacharya, D Roy, S Chatterjee, A Chakraborty, D Banerjee, A Ganguly, S Nanda and P Rajak. Contamination of textile dyes in aquatic environment: Adverse impacts on aquatic ecosystem and human health, and its management using bioremediation. *Journal of Environmental Management* 2024; **353**, 120103.

[38] M Al Kausor and D Chakrabortty. Polyaniline (PANI) grafted hierarchical heterostructure nanocomposites for photocatalytic degradation of organic pollutants in wastewater: A review. *Surfaces and Interfaces* 2022; **31**, 102079.

[39] CW Siao, HL Chen, LW Chen, JL Chang, TW Yeh and CC Chen. Controlled hydrothermal synthesis of bismuth oxychloride/bismuth oxybromide/bismuth oxyiodide composites exhibiting visible-light photocatalytic degradation of 2-hydroxybenzoic acid and crystal violet. *Journal of Colloid and Interface Science* 2018; **526**, 322-336.

[40] T Jia, J Yang, Y Zhang, L Ji, Y Chen, D Wang, J Wu, Y Qi and J Zhai. Facet-dependent flower-like BiOBr with exposed the (0 0 1) and (0 1 0) facets for enhanced charge carrier transfer and photocatalytic oxidation activity. *Chemical Physics Letters* 2020; **760**, 138010.

[41] L Lu, MY Zhou, L Yin, GW Zhou, T Jiang, XK Wan and HX Shi. Tuning the physicochemical property of BiOBr via pH adjustment: Towards an efficient photocatalyst for degradation of bisphenol A. *Journal of Molecular Catalysis A: Chemical* 2016; **423**, 379-385.

[42] Z Zhang, H Zhou, C Jiang and Y Wang. Molecularly imprinted polymer functionalized flower-like BiOBr microspheres for photoelectrochemical sensing of chloramphenicol. *Electrochimica Acta* 2020; **344**, 136161.

[43] Z Sun, B Mei, H Zhou, S Qin and H Zhang. Effect of film thickness and morphology on photoelectrochemical performance of (001) orientated BiOBr thin films prepared via mist CVD. *Ceramics International* 2022; **48(17)**, 25521-25527.

[44] X Xiong, L Ding, Q Wang, Y Li, Q Jiang and J Hu. Synthesis and photocatalytic activity of BiOBr nanosheets with tunable exposed {0 1 0} facets. *Applied Catalysis B: Environmental* 2016; **188**, 283-291.

[45] Y Mi, H Li, Y Zhang, N Du and W Hou. Synthesis and photocatalytic activity of BiOBr nanosheets with tunable crystal facets and sizes. *Catalysis Science & Technology* 2018; **8(10)**, 2588-2597.

[46] HP Lin, WW Lee, ST Huang, LW Chen, TW Yeh, JY Fu and CC Chen. Controlled hydrothermal synthesis of $PbBiO_2Br$/BiOBr heterojunction with enhanced visible-driven-light photocatalytic activities. *Journal of Molecular Catalysis A: Chemical* 2016; **417**, 168-183.

[47] F Akman, MR Kaçal, H Polat, G Aktas, A Gultekin and O Agar. A comparative study on the nuclear shielding properties of $BiBr_3$ and PbSO4 incorporated composites. *Journal of Physics and Chemistry of Solids* 2021; **152**, 109978.

[48] KL Li, WW Lee, CS Lu, YM Dai, SY Chou, HL Chen, HP Lin and CC Chen. Synthesis of BiOBr, Bi_3O_4Br, and $Bi_{12}O_{17}Br_2$ by controlled hydrothermal method and their photocatalytic properties. *Journal of the Taiwan Institute of Chemical Engineers* 2014; **45(5)**, 2688-2697.

[49] H Xu, Z Xu, J Zhou, G Yan, X Li and S Zhuo. Hydrothermal fabrication of BiOBr/magnetic reduced graphene oxide composites with efficient visible light photocatalytic activity. *Ceramics International* 2019; **45(12)**, 15458-15465.

[50] HL Chen, WW Lee, WH Chung, HP Lin, YJ Chen, YR Jiang, WY Lin and CC Chen. Controlled

hydrothermal synthesis of bismuth oxybromides and their photocatalytic properties. *Journal of the Taiwan Institute of Chemical Engineers* 2014; **45(4)**, 1892-1909.

[51] Z Cai, J Zhong and J Li. Ionic liquid assisted one-pot solvothermal preparation of BiOI/BiOBr heterojunctions with excellent photocatalytic activity. *Materials Letters* 2020; **271**, 127812.

[52] T Zhang, Q Yang, H Li, J Zhong, J Li and H Yang. Photocatalytic properties of BiOBr/g-C_3N_4 heterojunctions originated from S-scheme separation and transfer of interfacial charge pairs. *Optical Materials* 2022; **131**, 112649.

[53] D Wu, L Ye, S Yue, B Wang, W Wang, HY Yip and PK Wong. Alkali-Induced in Situ Fabrication of Bi_2O_4-Decorated BiOBr Nanosheets with Excellent Photocatalytic Performance. *The Journal of Physical Chemistry C* 2016; **120(14)**, 7715-7727.

[54] X Dai, S Yan, L Cui and L Shi. Fe(III) modified Bi_2O_4 nano-rods for boosting photocatalytic performance through interfacial charge transfer effect. *Ceramics International* 2020; **46(8)**, 11261-11267.

[55] Y Xing, F Tian, D Wu, X Yong, X Jin and G Ni. Facile synthesis of Z-scheme ZnMoO4/Bi_2O_4 heterojunction photocatalyst for effective removal of levofloxacin. *Inorganic Chemistry Communications* 2022; **143**, 109763.

[56] M Liu, G Liu, X Liu, X Wang, YL Chen, W Yang, C Gao, G Wang and Z Teng. One-pot synthesis of m-Bi_2O_4/Bi_2O_{4-x}/BiOCl with enhanced photocatalytic activity for BPA and CIP under visible-light. *Colloids and Surfaces A: Physicochemical and Engineering Aspects* 2022; **643**, 128772.

[57] S Yuan, X Liang, Y Zheng, Y Chu, X Ren, Z Zeng, G Nan, Y Wu and Y He. Enhanced piezocatalytic and piezo-photocatalytic dye degradation via S-scheme mechanism with photodeposited nickel oxide nanoparticles on PbBiO2Br nanosheets. *Journal of Colloid and Interface Science* 2024; **670**, 373-384.

[58] H Liu, B Wang, M Chen, H Zhang, J Peng, L Ding and W Wang. Simple synthesis of BiOAc/BiOBr heterojunction composites for the efficient photocatalytic removal of organic pollutants. *Separation and Purification Technology* 2021; **261**, 118286.

[59] S Li, P Wang, H Zhao, R Wang, R Jing, Z Meng, W Li, Z Zhang, Y Liu, Q Zhang and Z Li. Fabrication of black phosphorus nanosheets/BiOBr visible light photocatalysts via the co-precipitation method. *Colloids and Surfaces A: Physicochemical and Engineering Aspects* 2021; **612**, 125967.

[60] SM El-Sheikh, AB Azzam, RA Geioushy, FM El Dars and BA Salah. Visible-light-driven 3D hierarchical Bi_2S_3/BiOBr hybrid structure for superior photocatalytic Cr(VI) reduction. *Journal of Alloys and Compounds* 2021; **857**, 157513.

[61] AP Chowdhury and BH Shambharkar. Fabrication and characterization of BiOBr-$SnWO_4$ heterojunction nanocomposites with boosted photodegradation capability. *Chemical Engineering Journal Advances* 2020; **4**, 100040.

[62] Z Yao, H Sun, Y Hu, X Liu and Y Zhang. Construction of direct Z-scheme BPQDs-modified BiOBr thin film for enhanced photocatalytic performance under visible light irradiation. *Journal of Materiomics* 2021; **7(5)**, 1122-1130.

[63] Z Long, G Zhang, H Du, J Zhu and J Li. Preparation and application of BiOBr-Bi2S3 heterojunctions for efficient photocatalytic removal of Cr(VI). *Journal of Hazardous Materials* 2021; **407**, 124394.

[64] J Chen, Q Yang, J Zhong, J Li and C Burda. Microwave-assisted preparation of flower-like C60/BiOBr with significantly enhanced visible-light photocatalytic performance. *Applied Surface Science* 2021; **540**, 148340.

[65] Y Ling and Y Dai. Direct Z-scheme hierarchical WO_3/BiOBr with enhanced photocatalytic degradation performance under visible light. *Applied Surface Science* 2020; **509**, 145201.

[66] QY Tang, MJ Yang, SY Yang and YH Xu. Enhanced photocatalytic degradation of glyphosate over 2D CoS/BiOBr heterojunctions under visible light irradiation. *Journal of Hazardous Materials* 2021; **407**, 124798.

[67] X Wang, SH Teo, MR Shamsuddin and N Wid. Photocatalytic Degradation of Organic Pollutants and Microplastics Using Ag/TiO_2: Recent Advances in Mechanism, Synthesis and

Properties. *Water, Air, & Soil Pollution* 2025; **236(1)**, 30.

[68] HM El Sharkawy, AM Shawky, R Elshypany and H Selim. Efficient photocatalytic degradation of organic pollutants over TiO_2 nanoparticles modified with nitrogen and MoS_2 under visible light irradiation. *Scientific Reports* 2023; **13(1)**, 8845.

[69] F Gull, R Riaz, K Ansari and H Atiq. Examining the photo catalytic potency of annealed and un-annealed ZnO and nickel doped ZnO for degradation of organic pollutants in waste waters. *Scientific Reports* 2024; **14(1)**, 21828.

[70] A Yazdanbakhsh, A Eslami, M Massoudinejad, Z Gholami, M Sarafraz, Z Noorimotlagh, M Adiban and SA Mirzaee. Photocatalytic degradation and dechlorination mechanism of diclofenac using heterojunction Mn-doped tungsten trioxide (Mn-WO_3) nanoparticles under LED visible light from aqueous solutions. *Scientific Reports* 2024; **14(1)**, 29583.

[71] Q Han. Advances in preparation methods of bismuth-based photocatalysts. *Chemical Engineering Journal* 2021; **414**, 127877.

[72] Y Li, W Yin, N Yang, Y Li, C Zhu, L Liu, H Li and X Chen. Ag/AgCl/Bi_2O_3/$BiFeO_3$@zeolite for photocatalytic degradation of levofloxacin hydrochloride. *Materials Chemistry and Physics* 2023; **308**, 128189.

[73] J Liu, S Zhang and H Zhao. Fabricating visible-light photoactive 3D flower-like BiOCl nanostructures via a one-step solution chemistry method at room temperature. *Applied Surface Science* 2019; **479**, 247-252.

[74] L Hao, H Huang, Y Guo, X Du and Y Zhang. Bismuth oxychloride homogeneous phasejunction BiOCl/$Bi_{12}O_{17}Cl_2$ with unselectively efficient photocatalytic activity and mechanism insight. *Applied Surface Science* 2017; **420**, 303-312.

[75] Y Ao, J Bao, P Wang, C Wang and J Hou. Bismuth oxychloride modified titanium phosphate nanoplates: A new p-n type heterostructured photocatalyst with high activity for the degradation of different kinds of organic pollutants. *Journal of Colloid and Interface Science* 2016; **476**, 71-78.

[76] P Intaphong, A Phuruangrat, S Thongtem and T Thongtem. Sonochemical synthesis and characterization of BiOI nanoplates for using as visible-light-driven photocatalyst. *Materials Letters* 2018; **213**, 88-91.

[77] Y Huo, J Zhang, M Miao and Y Jin. Solvothermal synthesis of flower-like BiOBr microspheres with highly visible-light photocatalytic performances. *Applied Catalysis B: Environmental* 2012; **111-112**, 334-341.

[78] Y Long, Y Wang, D Zhang, P Ju and Y Sun. Facile synthesis of BiOI in hierarchical nanostructure preparation and its photocatalytic application to organic dye removal and biocidal effect of bacteria. *Journal of Colloid and Interface Science* 2016; **481**, 47-56.

[79] G Chen, M Zhu and X Wei. Photocatalytic properties of attached BiOCl-(001) nanosheets onto AgBr colloidal spheres toward MO and RhB degradation under an LED irradiation. *Materials Letters* 2018; **212**, 182-185.

[80] X Wang, C Zhou, L Yin, R Zhang and G Liu. Iodine-deficient BiOI nanosheets with lowered valence band maximum to enable visible light photocatalytic activity. *ACS Sustainable Chemistry & Engineering* 2019; **7(8)**, 7900-7907.

[81] L Zhang, X Yuan, H Wang, X Chen, Z Wu, Y Liu, S Gu, Q Jiang and G Zeng. Facile preparation of an Ag/$AgVO_3$/BiOCl composite and its enhanced photocatalytic behavior for methylene blue degradation. *RSC Advances* 2015; **5(119)**, 98184-98193.

[82] C Pan and S Jantasee. Fabrication of a novel microflower BiOCl composite incorporated with rosemary powder for enhanced oxygen vacancies and visible-light photocatalytic efficiency. *Journal of Alloys and Compounds* 2024; **1007**, 176393.

[83] J Wang and Z Zhang. Co-precipitation synthesis and photocatalytic properties of BiOCl microflowers. *Optik* 2020; **204**, 164149.

[84] AI Osman, N Mehta, AM Elgarahy, M Hefny, A Al-Hinai, AH Al-Muhtaseb and DW Rooney. Hydrogen production, storage, utilisation and environmental impacts: a review. *Environmental Chemistry Letters* 2022; **20(1)**, 153-188.

[85] K Huang, C Li, J Yang, R Zheng, W Wang and L Wang. Platinum nanodots modified Nitrogen-vacancies g-C_3N_4 Schottky junction for enhancing photocatalytic hydrogen evolution. *Applied Surface Science* 2022; **581**, 152298.

[86] A Hussain, J Hou, M Tahir, SS Ali, ZU Rehman, M Bilal, T Zhang, Q Dou and X Wang. Recent advances in BiOX-based photocatalysts to enhanced efficiency for energy and environment applications. *Catalysis Reviews* 2024; **66(1)**, 119-173.

[87] Z Wang, M Dou, X Liu, S Kang, L Kong, H Yang, Y Zhang, Y Chen, H Zhu and J Dou. Ternary Z-scheme α-Fe_2O_3/BiOBr/g-C_3N_4 photocatalyst for highly efficient hydrogen production coupled with diverse antibiotic degradation. *Journal of Environmental Chemical Engineering* 2024; **12(4)**, 113080.

[88] J Kosco, F Moruzzi, B Willner and I McCulloch. Photocatalysts based on organic semiconductors with tunable energy levels for solar fuel applications. *Advanced Energy Materials* 2020; **10(39)**, 2001935.

[89] G Salehi, M Bagherzadeh, R Abazari, M Hajilo and D Taherinia. Visible light-driven photocatalytic degradation of methylene blue dye using a highly efficient Mg–Al LDH@g-C_3N_4@Ag_3PO_4 nanocomposite. *ACS Omega* 2024; **9(4)**, 4581-4593.

[90] V Sodha, S Shahabuddin, R Gaur, I Ahmad, R Bandyopadhyay and N Sridewi. Comprehensive review on zeolite-based nanocomposites for treatment of effluents from wastewater. *Nanomaterials* 2022; **12(18)**, 3199.

[91] AY Kurenkova, AY Yakovleva, AA Saraev, EY Gerasimov, EA Kozlova and VV Kaichev. Copper-modified titania-based photocatalysts for the efficient hydrogen production under UV and visible light from aqueous solutions of glycerol. *Nanomaterials* 2022; **12(18)**, 3106.

[92] MS Alshammari, WH Hassan, MM Al-Zahiwat, H Osman, HA El-Sabban, MA Diab, Z Atamuratova, E Saitov and A Amari. Novel environmentally benign dual Z-scheme $SrTiO_3$/g-C_3N_4/ZnO heterojunction for efficient H2 evolution and polluted water treatment: Optimization, mechanism interpretations and toxicity assessment. *FlatChem* 2025; **50**, 100841.

[93] M Tan, C Yu, J Li, Y Li, C Tao, C Liu, H Meng, Y Su, L Qiao and Y Bai. Engineering of g-C_3N_4-based photocatalysts to enhance hydrogen evolution. *Advances in Colloid and Interface Science* 2021; **295**, 102488.

[94] R Li, JJ Peng, X Yu, Q Xi, J Qin, J Liu and J Wang. Fabrication of TiO_2/g-C_3N_4 S-scheme heterojunction photocatalysts for efficient hydrogen evolution. *Inorganic Chemistry Communications* 2025; **182**, 115665.

[95] EA Kozlova, AY Kurenkova, VS Semeykina, EV Parkhomchuk, SV Cherepanova, EY Gerasimov, AA Saraev, VV Kaichev and VN Parmon. Effect of titania regular macroporosity on the photocatalytic hydrogen evolution on $Cd_{1-x}Zn_xS/TiO_2$ catalysts under visible light. *ChemCatChem* 2015; **7(24)**, 4108-4117.

[96] F Dong, H Liu, L Qin, T Zhang, X Li and SZ Kang. Boosting the photocatalytic activity of ZnIn2S4-based photocatalyst for H_2 evolution using porous $ZnWO_4$ nanoflakelets as a cocatalyst. *New Journal of Chemistry* 2023; **47(28)**, 13177-13185.

[97] Y Xiang, G Hu, W Yang, F Huang, X Zhang, Q Xu, X Yuan, X Rao, S Zheng and G Wang. Facile construction of carbon-doped g-C_3N_4 using carbon quantum dots: Enhanced photocatalytic hydrogen evolution. *Ceramics International* 2025; **51(30)**, 62338-62349.

[98] X Liu, T Pei, L Yan, X Lei, T Zheng, X Ha and H Xu. Enhancing photocatalytic hydrogen evolution from water splitting over $CaTaO_2N$ via engineering the surface of a platinum cocatalyst. *New Journal of Chemistry* 2024; **48(32)**, 14298-14304.

[99] SZ Zhao, R Lu, Y Yang, Y Lu, RD Rodriguez and JJ Chen. Direct Z-scheme g-C_3N_4/TiO_2 heterojunction porous nanotubes: An ingenious synthesis strategy to enhance photocatalytic activity. *Journal of Environmental Chemical Engineering* 2023; **11(2)**, 109366.

[100] R Li, T Gao, Y Wang, Y Chen, W Luo, Y Wu, Y Xie, Y Wang and Y Zhang. Engineering of bimetallic Au–Pd alloyed particles on nitrogen defects riched g-C_3N_4 for efficient photocatalytic

hydrogen production. *International Journal of Hydrogen Energy* 2024; **63**, 1116-1127.

[101] R Jasrotia, A Verma, J Ahmed, V Khanna, SK Godara, M Fazil, T Ahmad, SM Alshehri, S Kumari and A Kandwal. Photocatalytic and electrocatalytic hydrogen production promoted by Nd/La substituted cobalt–nickel magnetic nanomaterials. *International Journal of Hydrogen Energy* 2024; **52**, 1217-1227.

[102] R Nawaz, M Saad, A Bahadur, S Iqbal, S Mahmood, A Zidan, MS Khan, R Liaquat, M Sohail and MT Alotaibi. Designing an innovative 2D/2D step scheme α-Fe_2O_3/BiOBr/MoS_2 ternary integrated heterojunction with unparalleled visible-light-induced remarkable photocatalytic H_2 evolution. *International Journal of Hydrogen Energy* 2025; **99**, 112-122.

[103] Z. Su et al., "Synergistic hydrazine-driven regulation and Mo/S co-doping to endow BiOBr with heterovalent molybdenum states and abundant oxygen vacancy defects for photocatalytic hydrogen evolution," J. Mater. Chem. A Mater., vol. 12, no. 41, pp. 28486–28502, 2024, doi: 10.1039/D4TA05641H.

[104] Z Su, B Wu, DH Kuo, L Chen, P Zhang, B Yang, X Wu, D Lu, J Lin and X Chen. Synergistic hydrazine-driven regulation and Mo/S co-doping to endow BiOBr with heterovalent molybdenum states and abundant oxygen vacancy defects for photocatalytic hydrogen evolution. *Journal of Materials Chemistry A* 2024; **12(41)**, 28486-28502.

[105] Q Chi, G Zhu, D Jia, W Ye, Y Wang, J Wang, T Tao, F Xu, G Jia, W Li and P Gao. Built-in electric field for photocatalytic overall water splitting through a TiO_2/BiOBr P–N heterojunction. *Nanoscale* 2021; **13(8)**, 4496-4504.

[106] A Zandi, RA Sene and F Rahmani. Design and construction of clinoptilolite-decorated BiOBr-TiO_2 heterojunction as efficient and affordable photocatalyst for herbicide contaminated wastewater splitting. *Scientific Reports* 2025; **15(1)**, 42720.

[107] L Shuai, L Tian, X Huang, J Dou, J Yu and X Chen. Enhanced charge carrier separation and stable photoelectrochemical water splitting via a high-performance $BiVO_4$/BiOBr Type-II heterojunction. *International Journal of Hydrogen Energy* 2024; **88**, 19-28.

[108] M Zhang, F Xie, L Zhang, X Jian, J Liu, X Zhang, Y Wang, R Li and C Fan. Efficient oxygen evolution photocatalyst of BiOBr: *In situ* light-induced formation of surface oxygen vacancies and application in water splitting. *Materials Letters* 2022; **321**, 132416.

[109] Y Fan, J Hu, T Li, S Xu, S Chen and H Yin. Enhanced photocatalytic hydrogen evolution through MoS_2 quantum dots modification of bismuth-based perovskites. *Chemical Communications* 2024; **60(8)**, 1004-1007.

[110] R Jia, J Deng, X Yang, R Xue, P Wang, X Bian and Q Wang. Probing the role of H-ZSM-5 zeolite in the hydrogen evolution performance of graphitic carbon nitride. *Journal of Environmental Chemical Engineering* 2023; **11(6)**, 111231.

[111] J Zhou, J Zhou, Z Hu and L Wang. Enhancement of adsorption and visible light photocatalytic activity of the Zn^{2+} doped BiOBr/PVPmodified microspheres for RhB. *Materials Science in Semiconductor Processing* 2019; **90**, 112-119.

[112] JA Arana-Trenado, D Ramírez-Ortega, A Serrano-Lázaro, A Hernández-Gordillo, SE Rodil and M Bizarro. Synergistic photocatalytic effect of BiOBr–BiOI heterojunctions due to appropriate layer stacking. *Dalton Transactions* 2022; **51(6)**, 2413-2427.

[113] AN Romanov, AI Serykh, EV Haula, DP Shashkin, VM Kogan, NN Rozhdestvenskaya, IB Krylov and VN Korchak. NIR photoluminescence of ZSM-5 and mordenite zeolites, containing low-valence bismuth exchange cations. *Microporous and Mesoporous Materials* 2022; **336**, 111875.

[114] K Badvi and V Javanbakht. Enhanced photocatalytic degradation of dye contaminants with TiO_2 immobilized on ZSM-5 zeolite modified with nickel nanoparticles. *Journal of Cleaner Production* 2021; **280**, 124518.

[115] S Varimalla, K Manda, S Boggala, RC Nappuni, S Inkollu, HP Aytam and V Akula. Effect of method of preparation of Ni and/or Cu supported on ZSM-5 catalysts for the aqueous phase hydrogenation of levulinic acid to γ-valerolactone. *Catalysis Today* 2024; **441**, 114916.

[116] AO Zaykovskaya, N Kumar, EA Kholkina, NS Li-Zhulanov, P Mäki-Arvela, A Aho, J Peltonen, M Peurla, I Heinmaa, BT Kusema, S Streiff and DY Murzin. Synthesis and physico-chemical characterization of Beta zeolite catalysts: Evaluation of catalytic properties in Prins cyclization of (−)-isopulegol. *Microporous and Mesoporous Materials* 2020; **302**, 110236.

[117] ML Bols, J Devos, HM Rhoda, D Plessers, EI Solomon, RA Schoonheydt, BF Sels and M Dusselier. Selective formation of α-Fe(II) sites on Fe-zeolites through one-pot synthesis. *Journal of the American Chemical Society* 2021; **143(39)**, 16243-16255.

[118] FS Faradilla, DT Nugroho, RE Hidayati, Nurlina, R Bayuaji, D Hartanto and H Fansuri. Optimization of SiO_2/Al_2O_3 ratio in the preparation of geopolymer from high calcium fly ash. *IOP Conference Series: Earth and Environmental Science* 2020; **616(1)**, 012051.

[119] E Pérez-Botella, S Valencia and F Rey. Zeolites in adsorption processes: State of the art and future prospects. *Chemical Reviews* 2022; **122(24)**, 17647-17695.

[120] GTM Kadja, NJ Azhari, S Mardiana, NTU Culsum and A Maghfirah. Recent advances in the development of nanosheet zeolites as heterogeneous catalysts. *Results in Engineering* 2023; **17**, 100910.

[121] K Sivagami, KV Kumar, P Tamizhdurai, D Govindarajan, M Kumar and I Nambi. Conversion of plastic waste into fuel oil using zeolite catalysts in a bench-scale pyrolysis reactor. *RSC Advances* 2022; **12(13)**, 7612-7620.

[122] B Bensafi, N Chouat and F Djafri. The universal zeolite ZSM-5: Structure and synthesis strategies. A review. *Coordination Chemistry Reviews* 2023; **496**, 215397.

[123] J Čejka, R Millini, M Opanasenko, DP Serrano and WJ Roth. Advances and challenges in zeolite synthesis and catalysis. *Catalysis Today* 2020; **345**, 2-13.

[124] X Liu, Z Hao, R Yu, X Zhang, Y Zhang and Y Zhang. Enhanced hydrophobic ZSM–5 with high capacity for toluene capture under high-humidity conditions. *Science of The Total Environment* 2023; **894**, 164919.

[125] Y Yang, H Zhu, X Xu, L Bao, Y Wang, H Lin and C Zheng. Construction of a novel lanthanum carbonate-grafted ZSM-5 zeolite for effective highly selective phosphate removal from wastewater. *Microporous and Mesoporous Materials* 2021; **324**, 111289.

[126] D Morankar, K Barhate and N Hatvate. ZSM-5 zeolite: Structural features, catalytic properties, and multidisciplinary applications in organic synthesis, material science, and environmental remediation. *Coordination Chemistry Reviews* 2026; **549**, 217245.

[127] S Radoor, J Karayil, A Jayakumar, J Parameswaranpillai and S Siengchin. Removal of methylene blue dye from aqueous solution using PDADMAC modified ZSM-5 zeolite as a novel adsorbent. *Journal of Polymers and the Environment* 2021; **29(10)**, 3185-3198.

[128] AS Al-Wasidi, FA Saad, S AlReshaidan and AM Naglah. Facile synthesis of ZSM-5/TiO_2/Ni novel nanocomposite for the efficient photocatalytic degradation of methylene blue dye. *Journal of Inorganic and Organometallic Polymers and Materials* 2022; **32(8)**, 3040-3052.

[129] ET Wahyuni, NP Diantariani, I Kartini and A Kuncaka. Enhancement of the photostability and visible photoactivity of ZnO photocatalyst used for reduction of Cr(VI) ions. *Results in Engineering* 2022; **13**, 100351.

[130] LQ Wang, HJ Li, JQ Diao, DD Hou, MM Qiang and LJ Chen. Photocatalytic performance of hierarchical metal-doped framework zeolite. *Inorganic Chemistry Communications* 2022; **140**, 109425.

[131] DC Park, S Moon, JH Song, H Kim, E Lee, YH Lim and DH Kim. Widening the operating window of Pt/ZSM-5 catalysts for efficient NO_x removal in H2-SCR: Insights from thermal aging. *Catalysis Today* 2024; **425**, 114318.

[132] XH Yan, P Li, H Yuan, W Huang, Z Hu and RT Yang. CO_2 capture by ZSM-5 with varied Si/Al molar ratios: Isothermal adsorption capacity of CO_2 vs dynamic CO_2 adsorption capacity. *Separation and Purification Technology* 2025; **354**, 129304.

[133] S Radoor, J Karayil, A Jayakumar, J Parameswaranpillai and S Siengchin. Efficient

removal of methyl orange from aqueous solution using mesoporous ZSM-5 zeolite: Synthesis, kinetics and isotherm studies. *Colloids and Surfaces A: Physicochemical and Engineering Aspects* 2021; **611**, 125852.

[134] Z Vaez and V Javanbakht. Synthesis, characterization and photocatalytic activity of ZSM-5/ZnO nanocomposite modified by Ag nanoparticles for methyl orange degradation. *Journal of Photochemistry and Photobiology A: Chemistry* 2020; **388**, 112064.

[135] R Sharma, S Barman and B Pal. Improved adsorption and photocatalytic activity of ZSM-5-loaded fly ash–TiO_2–Cu hybrid composites for crystal violet removal under visible-solar light irradiation. *Microporous and Mesoporous Materials* 2026; **400**, 113892.

[136] Z Zhao, N Wang, H Zhang, R Shang, J Xing, D Zhang and J Li. Fabrication of ZSM-5 zeolite supported TiO_2-NiO heterojunction photocatalyst and research on its photocatalytic performance. *Journal of Solid State Chemistry* 2022; **309**, 122895.

[137] L Xu, P Guo, J Xu, B Shen and Z Zhao. Regulation of TiO_2/ZSM-5 catalyst for enhanced photocatalytic toluene oxidation: Intensified light absorption, charge separation and toluene adsorption. *Colloids and Surfaces A: Physicochemical and Engineering Aspects* 2024; **690**, 133832.

[138] A Satriyatama, IDM Budi, HN Iman, H Susilo and WH Saputera. ZnO-incorporated ZSM-5 for photocatalytic CO_2 reduction into solar fuels under UV–visible light. *In*: Proceedings of the 2nd International Electronic Conference on Catalysis Sciences—A Celebration of Catalysts 10th Anniversary, Basel, Switzerland. 2021.

[139] H Li, Y Zhang, J Diao, M Qiang and Z Chen. Synthesis and Photocatalytic Activity of Hierarchical Zn-ZSM-5 Structures. *Catalysts* 2021; **11(7)**, 797.

[140] Y Jia, Y Zhang, Y Huang, L Chen, H Qin, Y Zhang and H Cui. CdS/PANI/ZSM-5 hollow spheres: A photocatalyst for efficient SBX degradation. *Journal of Molecular Liquids* 2023; **370**, 121019.

[141] N Karimah, AA Mahardika, WP Utomo, AI Rozafia, PAI Afifah, HY Chung, Z Zhu and D Hartanto. Preparation of titanium dioxide/graphitic carbon nitride heterostructure anchored on hierarchical ZSM-5 for synergistic adsorptive and photocatalytic dye degradation. *Journal of Molecular Structure* 2025; **1335**, 141968.

[142] W Wang, D Zhang, P Sun, Z Ji and J Duan. High efficiency photocatalytic degradation of indoor formaldehyde by Ag/g-C_3N_4/TiO_2 composite catalyst with ZSM-5 as the carrier. *Microporous and Mesoporous Materials* 2021; **322**, 111134.

[143] J Kianička, G Čík, F Šeršeň, I Špánik, R Sokolík and J Filo. Photo-reduction of CO_2 by VIS light on polythiophene-ZSM-5 zeolite hybrid photo-catalyst. *Molecules* 2019; **24(5)**, 992.

[144] B Divband, A Jodaie and M Khatmian. Enhancement of photocatalytic degradation of 4-nitrophenol by integrating Ag nanoparticles with ZnO/HZSM-5 nanocomposite. *Iranian Journal of Catalysis* 2019; **9(1)**, 63-70.

[145] C Wang, X Liang, L Wang, Q Yu, F Du, S Liu, X Yao and D Zhai. Multicomponent modification of nano-TiO_2 with defective ZSM-5, CuO and Ag for enhanced photocatalytic and antibacterial performance. *Journal of Photochemistry and Photobiology A: Chemistry* 2026; **472**, 116787.

[146] N Aghajari, Z Ghasemi, H Younesi and N Bahramifar. Synthesis, characterization and photocatalytic application of Ag-doped Fe-ZSM-5@TiO_2 nanocomposite for degradation of reactive red 195 (RR 195) in aqueous environment under sunlight irradiation. *Journal of Environmental Health Science and Engineering* 2019; **17(1)**, 219-232.

[147] GWA Nyakairu, PM Kapanga, M Ntale, SN Lusamba, RM Tshimanga, A Ammari and Z Shehu. Synthesis, characterization and application of Zeolite/Bi2O3 nanocomposite in removal of Rhodamine B dye from wastewater. *Cleaner Water* 2024; **1**, 100004.

[148] G Dashtpeyma and SR Shabanian. Efficient photocatalytic oxidative desulfurization of liquid petroleum fuels under visible-light irradiation using a novel ternary heterogeneous $BiVO_4$-CuO/modified natural clinoptilolite zeolite. *Journal of Photochemistry and Photobiology A: Chemistry* 2023; **445**, 115024.

[149] D Morankar, K Barhate and N Hatvate. ZSM-5 zeolite: Structural features, catalytic properties, and multidisciplinary applications in organic synthesis, material science, and environmental remediation. *Coordination Chemistry Reviews* 2026; **549**, 217245.

[150] Z Tian, TS Chee, R Meng, Y Hao, X Zhou, B Ma, L Zhu, T Duan and C Xiao. Incipient wetness impregnation to prepare bismuth-modified all-silica beta zeolite for efficient radioactive iodine capture. *Environmental Functional Materials* 2022; **1(1)**, 92-104.

[151] R Boudraa, D Talantikite-Touati, A Souici, A Djermoune, A Saidani, K Fendi, A Amrane, JC Bollinger, HN Tran, A Hadadi and L Mouni. Optical and photocatalytic properties of TiO_2–Bi_2O_3–CuO supported on natural zeolite for removing Safranin-O dye from water and wastewater. *Journal of Photochemistry and Photobiology A: Chemistry* 2023; **443**, 114845.

[152] M Zhang, X Sun, C Wang, Y Wang, Z Tan, J Li and B Xi. Photocatalytic degradation of rhodamine B using $Bi_4O_5Br_2$-doped ZSM-5. *Materials Chemistry and Physics* 2022; **278**, 125697.

[153] Y Shi, L Wang, S Dong, X Miao, M Zhang, K Sun, Y Zhang and J Sun. Wool-ball-like BiOBr@ZnFe-MOF composites for degradation organic pollutant under visible-light: Synthesis, performance, characterization and mechanism. *Optical Materials* 2022; **131**, 112580.